

Interplay between magnetism, superconductivity, and orbital order in a 5-pocket model for iron-based superconductors – a parquet renormalization group study

Laura Classen^{1,2}, Rui-Qi Xing², Maxim Khodas^{3,4} and Andrey V Chubukov²

¹ *Institut für Theoretische Physik,
Universität Heidelberg, 69120 Heidelberg, Germany,*

² *School of Physics and Astronomy,
University of Minnesota, Minneapolis, MN 55455, USA,*

³ *Department of Physics and Astronomy,
University of Iowa, Iowa City, IA 52242, USA,*

⁴ *Racah Institute of Physics,
The Hebrew University, Jerusalem 91904, Israel*

We report the results of the parquet renormalization group (RG) analysis of the phase diagram of the most general 5-pocket model for Fe-based superconductors. We use as an input the orbital structure of excitations near the five pockets made out of d_{xz} , d_{yz} , and d_{xy} orbitals and argue that there are 40 different interactions between low-energy fermions in the orbital basis. All interactions flow under RG, as one progressively integrates out fermions with higher energies. We find that the low-energy behavior is amazingly simple, despite the large number of interactions. Namely, at low-energies the full 5-pocket model effectively reduces either to a 3-pocket model made of one d_{xy} hole pocket and two electron pockets, or a 4-pocket model made of two d_{xz}/d_{yz} hole pockets and two electron pockets. The leading instability in the effective 4-pocket model is a spontaneous orbital (nematic) order, followed by s^{+-} superconductivity. In the effective 3-pocket model orbital fluctuations are weaker, and the system develops either s^{+-} superconductivity or stripe SDW. In the latter case, nematicity is induced by composite spin fluctuations.

Introduction. The interplay between superconductivity, magnetism, and nematicity is the key physics of Fe-based superconductors (FeSCs) [1–6]. In some FeSCs, e.g., 1111 and 122 systems, undoped materials display a stripe magnetic order below a certain T_N and a nematic order at slightly higher temperatures, while superconductivity emerges upon doping, when magnetic order gets weaker. In other systems, like 111 LiFeAs and 11 FeSe, superconductivity emerges without long-ranged magnetism already in undoped systems. Besides, FeSe displays an orbital order above the superconducting (SC) T_c [7]. The issue for the theory is to understand whether these seemingly different behaviors can be understood within the same framework.

In this communication we report the results of our analysis, which connects different classes of FeSCs. We study the competition between superconductivity, magnetism, and nematicity in the most generic five-pocket (5p) model for FeSCs with full orbital content of low-energy excitations. To do this, we use the machinery of analytical parquet renormalization group (pRG) [8]. This approach, along with complementary numerical functional RG [9–12], has been argued [4, 9–17] to be the most unbiased way to analyze competing orders in an itinerant electron system.

The 5p model consists of three hole pockets, of which two are centered at $\Gamma = (0,0)$ in the 1Fe Brillouin zone and one is centered at $M = (\pi, \pi)$, and two electron pockets centered at $Y = (0, \pi)$ and $X = (\pi, 0)$ (see the right panel in Fig. 1). The two Γ -centered hole pockets are made out of d_{xz} and d_{yz} orbitals, the hole pocket at M is made out of d_{xy} orbitals. The electron pockets are

made out of $d_{xz}(d_{yz})$ and d_{xy} orbitals [18, 19].

For such an electronic configuration, there are 40 different 4-fermion interaction terms, allowed by C_4 symmetry [20] (without the hole pocket at M , this number is 30 [21]). If one departs from the model with only local interactions, the bare values of all 40 interactions are linear combinations of inter- and intra-orbital Hubbard and Hund terms U , U' , J and J' . However, the 40 interactions flow to different values under pRG, which implies that the system self-generates non-local interactions. The flow of the interactions is obtained by solving differential equations that encode series of coupled vertex renormalizations. The running interactions are then used as input to determine susceptibilities in different channels. This way one can monitor a simultaneous build-up of different correlations taking into account their mutual feedback, which turns out to be crucial in our study.

The main result of pRG analysis is the emergent universality. It means that 40 microscopic interactions flow towards a *limited number* of fixed trajectories (FT), where the ratios of different interactions become universal numbers. Each fixed trajectory has a basin of attraction in the space of bare interaction parameters. This allows us to explain the rich behaviors of the different FeSCs within a unifying description. In practical terms a simultaneous build-up of different correlations holds in the window of energies between a fraction of W and a scale comparable to the Fermi energy, E_F . At smaller energies, interactions in different channels evolve independent on each other. The range between W and E_F should be wide enough, otherwise the pRG flow ends before the system reaches one of the FTs [22].

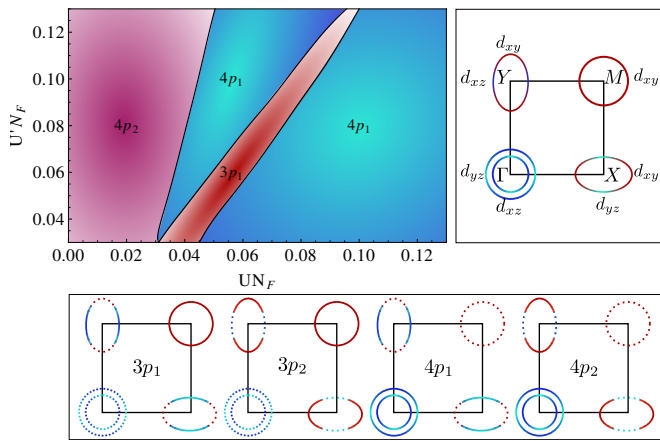


FIG. 1: Upper panel: Right – main orbital content of excitations near Fermi surfaces (presented by different colors). Left – regions of different system behavior of the full 5-pocket model, indicated by the type of the effective model. In the ranges marked $3p_{1,2}$, the dominant interactions at low energies are within the subset of the two electron pockets and the $M = (\pi, \pi)$ -hole pocket. In the ranges marked $4p_{1,2}$, the dominant interactions are between fermions near the Γ -centered hole pockets and electron pockets. The index 1,2 distinguishes if interactions involving d_{xz}/d_{yz} or d_{xy} orbital components on the electron pockets are dominant. For illustrative purposes, the bare model is set to have local Hubbard and Hund interactions – intraorbital U , interorbital U' , J and J' . We set $J = 0.025/N_F$, $J' = 0.03/N_F$, where N_F is the density of states on the FSs (assumed to be equal on all FSs for simplicity), and varied U and U' as two independent parameters. Lower panel: Graphic representations of $3p_{1,2}$ and $4p_{1,2}$ models. Fermionic states, for which interactions become the largest in the process of pRG flow, are shown by solid lines.

Summary of our results. We found four stable FTs. For the first two stable FTs, the interactions within the subset of the two Γ -centered hole pockets and the two electron pockets become dominant, i.e., the 5p model effectively reduces to the four-pocket model (4p). For the other two stable FTs, the 5p model reduces to an effective 3-pocket model (3p) consisting of two electron pockets and the M -hole pocket. On each of two stable 4p FTs or 3p FTs the system behavior is described by an even simpler effective model because interactions involving fermions from either d_{xz}/d_{yz} or d_{xy} orbitals become dominant. We label these models as $4p_1$, $3p_1$, and $4p_2$, $3p_2$, respectively. We illustrate the four cases and present the phase diagram in Fig. 1. We then computed susceptibilities in different channels [23]. We found that the interplay between spin-density-wave (SDW) magnetism and superconductivity is the same in all four effective models. Namely, the SDW susceptibility is the largest at intermediate energies and pushes SC and orbital susceptibilities up. However, in the process of the pRG flow the SC susceptibility overtakes the SDW one, and the feedback from SC fluctuations halts the increase of the SDW susceptibility (see Fig. 3(b)). As a consequence, already

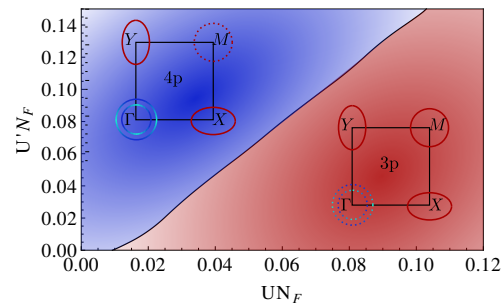


FIG. 2: Two different regions of system behavior indicated by fixed trajectories of the pRG flow for the toy model with electron pockets made entirely of d_{xy} , for different values of U, U' (treated as two independent parameters) and $J = J' = 0.03/N_F$. In the region labeled as 3p the interactions within the subset of the two electron pockets and the $M = (\pi, \pi)$ -hole pocket become dominant at low energies. In the region labeled as 4p interactions involving fermions from the two Γ -centered hole pockets and the two electron pockets become dominant.

the undoped system develops superconductivity rather than SDW magnetism, if indeed the pRG flow runs over a wide enough range of energies. This result could not be obtained within RPA and is entirely due to the feedback from increasing SC fluctuations on the SDW channel. In all cases superconductivity is of s^{+-} type, with sign change between the gaps on hole and electron pockets. In 4p models the susceptibility towards C_4 -breaking orbital order also grows, and its exponent is larger than that for superconductivity [4], i.e., the system first develops a spontaneous orbital order. In 3p models orbital fluctuations are much weaker, and orbital order does not have enough “space” to develop.

We found that SDW magnetism does develop before superconductivity and/or orbital order if the FT is not reached within the range of pRG flow. The type of SDW order is different for the 3p and the 4p models. In 3p models SDW order is a C_4 -breaking stripe order [24, 25], while in 4p models it is C_4 preserving double-Q order [26, 27] (a symmetric combination of $(\pi, 0)$ and $(0, \pi)$ magnetic orders). This last result, in combination with pRG, implies a clear separation between the magnetic and orbital scenario for nematicity in FeSCs. Namely, in 4p models, the SDW scenario for Ising-nematic order does not work because double-Q SDW preserves the symmetry between X and Y directions, and, simultaneously, orbital fluctuations are strong. In 3p models, orbital fluctuations are weak, and, simultaneously, SDW *stripe* fluctuations favor vestigial Ising-nematic spin order [28].

In the remainder of this Letter we present the details of our study. The full analysis of the set of 40 pRG equations is quite involved, so to demonstrate the separation into 4p or 3p behavior at low energies, we first analyze a toy model, in which we approximate the orbital composition of the two electron pockets as pure d_{xy} . We then extend the analysis to the full 5-pocket model.

Toy model with d_{xy} electron pockets. As

we said, the kinetic term describes fermionic excitations around the five Fermi surfaces, i.e. $H = H^\Gamma + H^X + H^Y + H^M$. The symmetry-allowed interaction terms contain 14 interactions U_i within the subset of the two electron and the two Γ -centered hole pockets and 7 interactions U_{in} involving fermions near the M -hole pocket, so the total number of the interactions is 21. We present the Hamiltonian and the full set of pRG equations for a generic dispersion near hole and electron FSs in the Supplementary Material (SM). The pRG analysis shows that six interactions flow to zero and five increase with smaller exponents than the other ten. The pRG flow of the remaining ten interactions determines the FTs. We show these ten interactions in the inset of Fig. 3(a). The pRG equations for these interactions are ($u_i = U_i N_F$)

$$\begin{aligned}
\dot{u}_1 &= u_1^2 + u_3^2, & \dot{u}_{1n} &= u_{1n}^2 + u_{3n}^2 & (1) \\
\dot{u}_2 &= 2u_2(u_1 - u_2), & \dot{u}_{2n} &= 2u_{2n}(u_{1n} - u_{2n}) \\
\dot{u}_3 &= 2u_3(2u_1 - u_2 - u_5) - 2u_3u_4 - u_{3n}u_{5n} \\
\dot{u}_{3n} &= 2u_{3n}(2u_{1n} - u_{2n} - u_5) - u_{3n}u_{4n} - 2u_3u_{5n} \\
\dot{u}_4 &= -2u_4^2 - 2u_3^2 - 2u_{5n}^2, & \dot{u}_{4n} &= -u_{4n}^2 - 2u_{3n}^2 - 2u_{5n}^2 \\
\dot{u}_5 &= -2u_5^2 - 2u_3^2 - u_{3n}^2, \\
\dot{u}_{5n} &= -2u_4u_{5n} - u_{4n}u_{5n} - 2u_3u_{3n}
\end{aligned}$$

The derivatives are with respect to $L = \log W/E$, where E is the running scale.

We searched for FTs of Eq. (S17) by selecting one divergent interaction (specifically u_1 or u_{1n}), writing other interactions as $u_i = \gamma_i u_1$, $u_{in} = \gamma_{in} u_1$ (or $u_i = \gamma_i u_{1n}$, $u_{in} = \gamma_{in} u_{1n}$), and solving the set of equations for L -independent γ_i, γ_{in} . We found two stable FTs: one with

$$u_1 = \frac{1}{1 + \gamma_3^2} \frac{1}{L_0 - L}, \quad (2)$$

and $\gamma_{in} = \gamma_2 = 0$, $\gamma_3 = \pm\sqrt{15}$, $\gamma_4 = \gamma_5 = 3$, and the other with

$$u_{1n} = \frac{1}{1 + \gamma_{3n}^2} \frac{1}{L_0 - L} \quad (3)$$

and $\gamma_1 = \gamma_2 = \gamma_3 = \gamma_4 = \gamma_{2n} = \gamma_{5n} = 0$, $\gamma_{3n} = \pm(3 + 2\sqrt{6})$, $\gamma_{4n} = 2\gamma_5 = -\sqrt{6}$. In Eqs. (2), (3) L_0 is the scale at which interactions diverge and the system develops a long-range order, as we show below. For the first stable FT all γ_{in} involving the M pocket vanish, so the 5-pocket model effectively reduces to the 4p model. For the second stable FT the situation is the opposite – interactions involving the two Γ -centered hole pockets vanish compared to other interactions, i.e., the 5p model effectively reduces to the 3p model. We checked the stability of the 4p FT and the 3p FT by expanding around them and verified that all eigenvalues are negative. Whether the system flows to one FT or the other is determined by the bare values of the interactions (see Fig.2).

We next use the running interactions as inputs and compute the susceptibilities in different channels, χ_j .

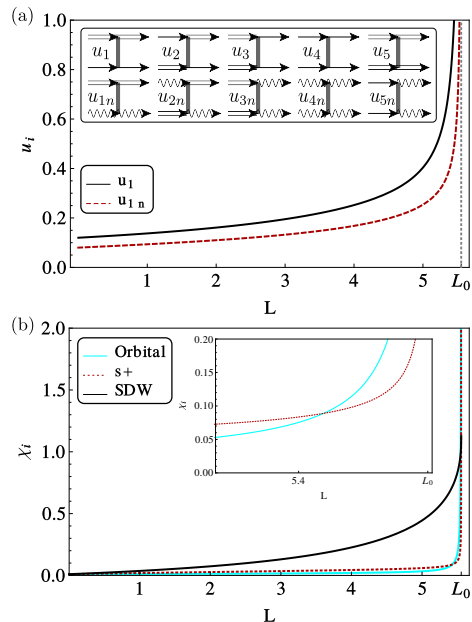


FIG. 3: (a) Representative RG flow towards the 4p FT in the toy model for the interactions u_1 and u_{1n} . The inset shows the 10 relevant interactions of the toy model, where double lines represent electron pockets, wavy lines the M -centered hole pocket and solid single lines the Γ -centered hole pockets. Bare values are $U = 0.08/N_F$, $U' = 0.12/N_F$, $J = J' = 0.03/N_F$. The RG parameter L is $\log W/E$, where W is the bandwidth and E is running energy/temperature. The system undergoes an instability into an ordered state (SDW, SC, or orbital order) at $L = L_0$. (b) Corresponding flow of the SDW, SC s^{+-} and orbital susceptibilities. Near $L = L_0$ the SC and the orbital susceptibilities keep increasing, while the SDW susceptibility remains finite. The inset shows orbital and SC susceptibilities at the end of the flow.

We describe the computational procedure in the SM and here list the results. The potentially divergent parts of the susceptibilities in SC and SDW channels are $\chi_i \propto (L_0 - L)^{2\beta_i - 1}$ ($i = \text{SDW, SC}$). Along 4p FT and 3p FT, the exponents are $\beta_{SDW}^{(4p)} = 0.30$, $\beta_{SC}^{(4p)} = 0.86$, $\beta_{SDW}^{(3p)} = 0.43$, $\beta_{SC}^{(3p)} = 0.72$. We see that in both cases $\beta_{SC} > 1/2$ while $\beta_{SDW} < 1/2$, i.e. χ_{SC} diverges at $L = L_0$, while χ_{SDW} remains finite, despite that it was the largest at the beginning of the pRG flow. This implies that the system develops SC order but not SDW order. We show the flow of the susceptibilities in Fig. 3(b). For both 4p and 3p models, we found that the largest $\beta_{SC} > 0$ corresponds to the s^{+-} gap structure, with opposite sign of the gap on hole and electron pockets [29]

We also analyzed the susceptibility χ_P in the d -wave Pomeranchuk channel. An instability in this channel leads to spontaneous orbital order [4, 6], i.e., non-equal densities of fermions on d_{xz} and d_{yz} orbitals. For the 4p model we found that $\beta_P^{(4p)} = 1$ is larger than $\beta_{SC}^{(4p)}$, i.e., orbital order can precede the SC transition [4]. We found no d_{xz}/d_{yz} orbital order for the 3p model because the electron and the M pockets have d_{xy} character [30].

Full 5-pocket model. The analysis of the full 5-pocket model with d_{xz}/d_{xy} and d_{yz}/d_{xy} orbital content of the electron pockets is more involved as one has to analyze the set of 40 coupled differential equations for the interactions (see SM). We searched for FTs with the same procedure as in the toy model. Amazingly enough, we found much the same behavior. Namely, the 5p model effectively becomes either a 4p or a 3p model. The new feature, not present in the toy model, is that in each case there are now two stable FTs, on which the system behavior is described by even more restricted $3p_{1,2}$ and $4p_{1,2}$ models. For $3p_1$ and $4p_1$ models interactions involving fermions from d_{xz} (d_{yz}) orbitals on the electron pockets become dominant, for $3p_2$ and $4p_2$ models interactions of d_{xy} orbitals on the electron pockets become dominant. We verified that these four FTs are stable with respect to small deviations. We show the phase diagram in Fig. 1.

The interplay between SDW and SC is the same in all four effective models and is similar to that in the toy model. Namely, the SDW susceptibility is the largest at the beginning, but in the process of the flow SC susceptibility diverges faster, and the feedback from SC fluctuations halts the growth of SDW susceptibility. As a result, even at zero doping the system develops s^{+-} SC order but no SDW order. Orbital fluctuations are, however, different in 4p and 3p models, again in similarity to the toy model. If the pRG flow is towards $4p_1$ or $4p_2$ models, orbital fluctuations also get strong and χ_P diverges with the largest exponent, i.e., the system develops a spontaneous orbital order prior to SC [32]. If the flow is towards 3p model, orbital fluctuations are much weaker and do not develop for not too large W/E_F . If E_F is larger than $E_0 \sim W e^{-L_0}$, the pRG flow ends before χ_{SC} and/or χ_P wins over χ_{SDW} . In this situation, the system develops SDW order at smaller doping and SC order at larger dopings [22]. For the 4p model an SDW order is a double-Q order, maintaining the symmetry between X and Y directions [26, 27], while for the 3p model SDW order is a stripe, breaking this symmetry. [24, 25]. Combining this with pRG results, we find that, if the pRG flow is towards one of the two 4p models, the nematicity emerges as a spontaneous orbital order. If the flow is towards one of the 3p models, the nematicity emerges due to stripe fluctuations as a composite Ising-nematic spin order.

Applications to FeSCs. Our results have several implications for FeSCs. First, the pRG analysis shows that SC order may develop instead of long-ranged magnetism already in undoped materials, not only when SDW order is destroyed by doping. This is consistent with the behavior in LiFeAs and FeSe [33]. In systems with smaller regions of the pRG flow (larger bare inter-

actions or larger E_F) SDW order develops first, and SC develops only upon doping. Second, pRG analysis shows that in 4p models orbital order develops first, SC develops at a lower T , and SDW order does not develop down to $T = 0$. This is consistent with the observed behavior in FeSe at ambient pressure [7]. The third result is the separation between orbital and magnetic scenarios for nematicity in 4p and 3p models. Whether the system flows towards 3p or 4p effective model at low energies depends on the microscopic Hubbard and Hund parameters (see Figs. 1, 2) as well as the parameters of fermionic dispersions (see SM).

Conclusions. In this Letter we analyzed the competition between SDW, SC, and orbital order in the full 5-pocket model for FeSCs. We used pRG techniques and included into consideration the orbital composition of hole and electron pockets in terms of d_{xz} , d_{yz} , and d_{xy} orbitals. The total number of symmetry-allowed interactions between low-energy fermions is 40, yet we found the system behavior is amazingly simple – depending on initial values of the interactions and quasiparticle masses the system flows to one of four stable FTs. For two of these FTs, the system behavior at low energies is the same as if the the M-pocket was absent (4p model), for the other two the system behavior is the same as if the two Γ -centered hole pockets were absent (3p model). In all cases s^{+-} SC wins over SDW if E_F is small enough, and SDW wins if E_F is larger. In the parameter range where the pRG flow is towards the effective 4p model, the system develops spontaneous orbital order, which then is the origin of nematicity. When the pRG flow is towards the effective 3p model, a spontaneous orbital order does not develop, and nematicity is associated with Ising-nematic spin order. The phase diagram in Fig. 1 describes the behavior found in all four families of FeSCs – 1111, 122, 111 and 11 systems, and in this respect our findings provide a unified description of the competition between SDW, SC, and orbital orders in all FeSCs.

We acknowledge with thanks the discussions with E. Berg, L. Boeri, S. Borisenko, P. Coleman, R. Fernandes, C. Honerkamp, D-H Lee, W. Metzner, A. Nevedomsky, D. Podolsky, M. Scherer, Q. Si, R. Thomale, A-M Tremblay, O. Vafek, C. Varma, and Fa Wang. L.C. thanks the School of Physics and Astronomy of the University of Minnesota for hospitality during this work and acknowledges funding by the Studienstiftung des deutschen Volkes and the HGSFP at Heidelberg University. A.C. is supported by the Office of Basic Energy Sciences, U.S. Department of Energy, under award DE-SC0014402. MK is supported by the Israel Science Foundation ISF, Grant No. 1287/15 and NSF DMR-1506668.

[1] Fernandes, R. M. Chubukov, A. V. and Schmalian, J. Nature Phys. 10, 97 (2014); P. C. Canfield and S. L. Bud'ko, Annu. Rev. Condens. Matter Phys. 1, 27 (2010).

[2] Liang, S., Moreo, A. and Dagotto, E. Phys. Rev. Lett. 111, 047004 (2013).

[3] see, e.g., A.V. Chubukov, in "Iron-based Superconduc-

- tivity”, Springer Series in Materials Science, Vol. 211, pp. 255-329, (2015); Luca de’ Medici, *ibid* pp. 409-441, (2015).
- [4] A.V. Chubukov, M. Khodas, and R.M. Fernandes, arXiv:1602.05503.
- [5] Cvetkovic, V. and Tesanovic, Z., Phys. Rev. B 80, 024512 (2009);
- [6] Yamase, H. and Zeyher, R., Phys. Rev. B 88, 180502(R) (2013); Lee, C. C., Yin, W. G. and Ku, W. Phys. Rev. Lett. 103, 267001 (2009); Kruger, F. S., Kumar, J., Zanen, J. and van den Brink, Phys. Rev. B 79, 054504 (2009); Valenzuela, B., Bascones, E. and Calderon, M. J. Phys. Rev. Lett. 105, 207202 (2010). Lv, W. and Phillips, P., Phys. Rev. B 84, 174512 (2011); Lee, W.-C. and Phillips, P. W. Phys. Rev. B 86, 245113 (2012); Applegate, R., Singh, R. R. P., Chen, C.-C. and Devereaux, T. P. Phys. Rev. B 85, 054411 (2012); Stanev, V. and Littlewood, P. B., Phys. Rev. B 87, 161122(R) (2013); Dumitrescu, P. T., Serbyn, M., Scalettar, R. T., and Vishwanath, A, arXiv:1512:08523 (2015); Baek, S.-H., Efremov, D. V., Ok, J. M., Kim, J. S., van den Brink, J. and Buchner, B. Nat Mater 14, 210 (2015); Gallais, I. and Paul, I. Comptes Rendus Physique 17, 113-139 (2016); Wang, Z., and Nevidomskyy, A. H., Journal of Physics: Condensed Matter bf 27, 225602 (2015); Thorsmille, V. K., Khodas, M., Yin, Z.P., Zhang, C., Carr, S.V., Dai, P., and Blumberg, G., Phys. Rev. B 93, 054515 (2016)
- [7] Watson, M. D., Kim, T. K., Haghighirad, A. A., Davies, N. R., McCollam, A., Narayanan, A., Blake, S. F., Chen, Y. L., Ghannadzadeh, S., Schofield, A. J., Hoesch, M., Meingast, C., Wolf, T. and Coldea, A. I., Phys. Rev. B 91, 155106 (2015); Y. Suzuki, T. Shimojima, T. Sonobe, A. Nakamura, M. Sakano, H. Tsuji, J. Omachi, K. Yoshioka, M. Kuwata-Gonokami, T. Watashige, R. Kobayashi, S. Kasahara, T. Shibauchi, Y. Matsuda, Y. Yamakawa, H. Kontani, and K. Ishizaka, Phys. Rev. B 92, 205117 (2015); Zhang, Y., *et al.* arXiv: 1503.01556; Zhang, P. *et al.* Phys. Rev. B 91, 214503 (2015); Kothapalli, K. *et al.* arXiv:1603.04135 (2016); Fedorov, A., Yaresko, A, Kim, T. K., Kushnirenko, E. Haubold, E, Wolf, T., Hoesch, M., Gruneis, A., Buchner, B., and Borisenko S. preprint.
- [8] see e.g., A.T. Zheleznyak, V.M. Yakovenko, and I.E. Dzyaloshinskii, Phys. Rev. B 55, 3200 (1997) and references therein.
- [9] Metzner, W., Castellani, C. and Di Castro, C. Adv. Phys. 47, 317 (1998); Salmhofer M., Commun. Math. Phys. 194, 249 (1998).
- [10] Platt, C., Honerkamp, C., and Hanke, W., New J. Phys. 11, 055058 (2009);
- [11] Platt, C., Hanke, W. and Thomale, R., Advances in Physics 62, 453-562 (2013).
- [12] Yang, F., Wang, F., and Lee, D.-H., Phys. Rev. B 88, 100504 (2013).
- [13] LeHur, K. and Rice, T. M., Ann. Phys. 324, 1452 (2009).
- [14] Nandkishore, L., Levitov, L., and Chubukov, A.V., Nature Phys. 8, 158 (2012); Kiesel, M., Platt, C. Hanke, W., Abanin, D.A., and Thomale R., Phys. Rev. B 86, 020507 (2012).
- [15] Chubukov, A. V., Efremov, D. V. and Eremin, Phys. Rev. B 78, 134512 (2008)
- [16] D. Podolsky, H-Y. Kee, Y. B. Kim, Europhysics Letters 88, 17004 (2009); Maiti, S and Chubukov, A. V. Phys. Rev. B 82, 214515 (2010).
- [17] Yamakawa, Y., Onari, S., and Kontani, arXiv:1509.01161
- [18] see. e.g., Kemper, A. F., Maier, T. A., Graser, S., Cheng, H.-P., Hirschfeld, P. J. and Scalapino, D. J. New Journal of Physics 12, 073030 (2010) and references therein.
- [19] see, e.g., V. Brouet, M. Fuglsang Jensen, Ping-Hui Lin, A. Taleb-Ibrahimi, P. Le Fvre, F. Bertran, Chia-Hui Lin, Wei Ku, D. Colson, and A. Forget, Phys. Rev. B 86, 075123 (2012).
- [20] See Supplementary Material for detail. The 40 interactions involve pairs of fermions, each near either Γ , X , Y or M point. There are 4 additional interactions involving fermions near each of these points. These additional interactions do not affect the behavior near the four stable fixed trajectories that we found within the space of 40 couplings, as we explicitly verified. We neglect these additional interactions in our analysis.
- [21] Cvetkovic, V. and Vafeek, O., Phys. Rev. B 88, 134510 (2013). See also Fernandes, R. M. and Vafeek, O., Phys. Rev. B 90, 214514 (2014).
- [22] see e.g. S. Maiti, A. Chubukov, Phys. Rev. B, 82, 214515 (2010) for a detailed explanation
- [23] A similar procedure has been used in the RG studies of other problems: see, e.g., Metzner, W., Salmhofer, M., Honerkamp C., Meden, V., and Schoenhammer K., Rev. Mod. Phys. 84, 299 (2012) and references therein; Lemonik Y., Aleiner, I.L., and Fal’ko V.L., Physical Review B 85, 245451 (2012); Murray, J. M., and Vafeek, O., Phys. Rev. B 89, 201110(R) (2014).
- [24] Eremin, I. and Chubukov, A. V., Phys. Rev. B 81, 024511 (2010).
- [25] Chandra, P., Coleman, P., and Larkin, A. I., Phys. Rev. Lett. 64, 88, (1990); Fang, C., Yao, H., Tsai, W.-F., Hu, J. and Kivelson, S. A. Phys. Rev. B 77, 224509 (2008); Xu, C., Muller, M., and Sachdev, S., Phys. Rev. B 78, 020501(R) (2008).
- [26] R.M. Fernandes, M. Khodas, and A.V. Chubukov, in preparation.
- [27] M.N., Gastiasoro, I. Eremin, R.M. Fernandes, and B.M. Andersen, arXiv:1607.04711
- [28] R. M. Fernandes, A.V. Chubukov, J. Knolle, I. Eremin, and J. Schmalian, Phys. Rev. B 85, 024534 (2012).
- [29] For the 3p case, the subleading eigenfunction (smaller $\beta_{SC} > 0$) describes the orbital-antiphase state with the gap sign on the M pocket opposite to that on the other four pockets, see Yin, Z. P., Haule, K., and Kotliar, G., Nature Phys. 10, 845 (2014).
- [30] We call orbital order the symmetry breaking between d_{xz} and d_{yz} orbitals. Another C_4 - symmetry breaking term is the difference in the occupations of d_{xy} orbitals at X and Y in the 1FeBZ [31]. Such an order is present in our $3p_2$ model and $4p_2$ models.
- [31] R. M. Fernandes and O. Vafeek, Phys. Rev. B 90, 214514 (2014).
- [32] For the application of the full 4p model to FeSe see R. Xing, L. Classen, M. Khodas, and A.V. Chubukov, arXiv:1611.03912
- [33] SC not preceded by SDW already at zero doping has been detected in a fRG analysis of a 4-pocket model and contrasted with the reported lack of such tendency in 5-pocket models [34]. We argue that the outcome of the pRG flow is qualitatively the same in both cases, only in the 5-pocket model the SC susceptibility overcomes the SDW susceptibility at smaller energies, i.e. after a longer RG flow.

- [34] R. Thomale, C. Platt, W. Hanke, B. A. Bernevig, Phys. Rev. Lett. 106, 187003 (2011).
 [35] O. Vafek and A.V. Chubukov, in preparation.

Supplemental Material

I. 3-ORBITAL, 5-BAND MODEL

A. Kinetic part of the Hamiltonian

We use as an input the fact that the low-energy excitations near all 5 Fermi surfaces are composed out of three orbitals – d_{xz} , d_{yz} , and d_{xy} . We perform calculations in the 1-Fe unit cell and neglect the dispersion in the third direction and the processes with momentum non-conservation by (π, π) (the ones which hybridize the pockets).

One way to obtain the dispersion of low-energy excitations is to use the tight-binding model in the orbital basis, restrict with d_{xz} , d_{yz} , and d_{xy} orbitals, and expand around the high-symmetry points in the Brillouin zone, where different electron and hole pockets are located (cf. Fig. S1). Another way to obtain low-energy dispersions is to identify the symmetry properties around the Fermi level and construct the invariants to leading order in the deviations from the symmetry points [S21]. The two approaches are equivalent to quadratic order in the deviations near the centra of the pockets ($\Gamma = (0, 0)$ for two hole pockets, $M = (\pi, \pi)$ for the third hole pocket, and $X = (\pi, 0)$ and $Y = (0, \pi)$ for the two electron pockets). The effective low-energy Hamiltonian reads

$$H_0 = \sum_{\mathbf{k}, \sigma} \left[\psi_{\Gamma, \mathbf{k}, \sigma}^\dagger h_{\Gamma}(\mathbf{k}) \psi_{\Gamma, \mathbf{k}, \sigma} + \psi_{X, \mathbf{k}, \sigma}^\dagger h_X(\mathbf{k}) \psi_{X, \mathbf{k}, \sigma} + \psi_{Y, \mathbf{k}, \sigma}^\dagger h_Y(\mathbf{k}) \psi_{Y, \mathbf{k}, \sigma} + \psi_{M, \mathbf{k}, \sigma}^\dagger h_M(\mathbf{k}) \psi_{M, \mathbf{k}, \sigma} \right], \quad (\text{S1})$$

where

$$h_{\Gamma}(\mathbf{k}) = \begin{pmatrix} \epsilon_{\Gamma} + \frac{k^2}{2m_{\Gamma}} + ak^2 \cos 2\theta_k & ck \sin 2\theta_k \\ ck \sin 2\theta_k & \epsilon_{\Gamma} + \frac{k^2}{2m_{\Gamma}} + ak^2 \cos 2\theta_k \end{pmatrix}$$

$$h_{X/Y}(\mathbf{k}) = \begin{pmatrix} \epsilon_1 + \frac{k^2}{2m_1} \pm a_1 k^2 \cos 2\theta_k & -iv_{X/Y}(\mathbf{k}) \\ iv_{X/Y}(\mathbf{k}) & \epsilon_3 + \frac{k^2}{2m_3} \pm a_3 k^2 \cos 2\theta_k \end{pmatrix}$$

$$h_M(\mathbf{k}) = \epsilon_M - \frac{k^2}{2m_M} \quad (\text{S2})$$

where $v_X(k) = 2vk \sin \theta$, $v_Y(k) = 2vk \cos \theta$ and $\theta_k = \arctan \frac{k_y}{k_x}$. Here and below the term A/B (in, e.g., $h_{X/Y}$) means "either A or B". The spinors in Eq. (S1) are defined as $\psi_{\Gamma, \mathbf{k}, \sigma} = (d_{yz, \mathbf{k}, \sigma}, d_{xz, \mathbf{k}, \sigma})^T$, $\psi_{X, \mathbf{k}, \sigma} = (d_{yz, \mathbf{X}+\mathbf{k}, \sigma}, d_{xy, \mathbf{X}+\mathbf{k}, \sigma})^T$, $\psi_{Y, \mathbf{k}, \sigma} = (d_{xz, \mathbf{Y}+\mathbf{k}, \sigma}, d_{xy, \mathbf{Y}+\mathbf{k}, \sigma})^T$ and $\psi_{M, \mathbf{M}+\mathbf{k}, \sigma} = d_{xy, \mathbf{k}, \sigma}$. Below we shorten notations to $d_{yz, \mathbf{k}, \sigma} = d_{1, \mathbf{k}, \sigma}$, $d_{xz, \mathbf{k}, \sigma} = d_{2, \mathbf{k}, \sigma}$, $d_{yz, \mathbf{X}+\mathbf{k}, \sigma} = f_{1, \mathbf{k}, \sigma}$, $d_{xz, \mathbf{Y}+\mathbf{k}, \sigma} = f_{2, \mathbf{k}, \sigma}$, $d_{xy, \mathbf{X}+\mathbf{k}, \sigma} = f_{31, \mathbf{k}, \sigma}$, $d_{xy, \mathbf{Y}+\mathbf{k}, \sigma} = f_{32, \mathbf{k}, \sigma}$, and $d_{xy, \mathbf{k}, \sigma} = d_{3, \mathbf{k}, \sigma}$. In these notations, the

spinors are $\psi_{\Gamma, \mathbf{k}, \sigma} = (d_{1, \mathbf{k}, \sigma}, d_{2, \mathbf{k}, \sigma})^T$, $\psi_{X/Y, \mathbf{k}, \sigma} = (f_{1/2, \mathbf{k}, \sigma}, f_{31/32, \mathbf{k}, \sigma})^T$ and $\psi_{M, \mathbf{M}+\mathbf{k}, \sigma} = d_{3, \mathbf{k}, \sigma}$.

To make RG analysis more tractable we made several simplifications in Eq. (S2). For Γ -centered hole pockets we set $a = c$. Then the transformation from the orbital to the band basis is given by

$$\begin{pmatrix} d_{1, \mathbf{k}, \sigma} \\ d_{2, \mathbf{k}, \sigma} \end{pmatrix} = \begin{pmatrix} \cos \theta_k & \sin \theta_k \\ -\sin \theta_k & \cos \theta_k \end{pmatrix} \begin{pmatrix} c_{\mathbf{k}, \sigma} \\ d_{\mathbf{k}, \sigma} \end{pmatrix}, \quad (\text{S3})$$

and the dispersions of fermions $c_{\mathbf{k}, \sigma}$ and $d_{\mathbf{k}, \sigma}$ are isotropic in \mathbf{k} :

$$\epsilon_{c/d, \mathbf{k}, \sigma} = -\frac{k^2}{2m_{c/d}} \quad (\text{S4})$$

where $m_{c/d}^{-1} = m_{\Gamma}^{-1} \pm 2a$. The two hole Fermi surfaces are obviously circular. The fermionic Green's functions in the orbital representation are related to $G_{c/d}(i\omega, \mathbf{k}) = (i\omega - \epsilon_{c/d, \mathbf{k}} - \mu)^{-1}$ in the band representation as

$$G_{d_1, d_1}(i\omega, \mathbf{k}) = G_c(i\omega, \mathbf{k}) \cos^2 \theta + G_d(i\omega, \mathbf{k}) \sin^2 \theta$$

$$G_{d_2, d_2}(i\omega, \mathbf{k}) = G_c(i\omega, \mathbf{k}) \sin^2 \theta + G_d(i\omega, \mathbf{k}) \cos^2 \theta$$

$$G_{d_1, d_2}(i\omega, \mathbf{k}) = G_{d_2, d_1}(i\omega, \mathbf{k}) = [G_d(i\omega, \mathbf{k}) - G_c(i\omega, \mathbf{k})] \sin \theta \cos \theta \quad (\text{S5})$$

A third hole pocket arises around the M -point in the Brillouin zone. Here the transformation from orbital to band basis is trivial, because the spectral weight comes entirely from the d_{xy} orbital. The dispersion is given in Eq. (S2), and the corresponding Green's function is $G_M(i\omega, \mathbf{k}) = (i\omega + k^2/(2m_M) - \epsilon_M)^{-1}$. The presence of this hole pocket is material dependent and relatively small changes in the system parameters may sink this pocket below the Fermi level (at least at $k_z = 0$, when k_z dispersion is included). However, such a pocket is definitely present in, e.g., hole-doped $K_x\text{Ba}_{1-x}\text{Fe}_2\text{As}_2$ and LiFeAs , which motivates to include it into our model.

For electron pockets, the diagonalization of h_X (h_Y) gives two bands, of which only one crosses the Fermi level and forms the electron pocket around X (Y). The electron pockets at X and Y are related by C_4 symmetry, i.e. they map onto each other under a rotation by $\pi/2$. Due to the non-diagonal hybridization $v_{X/Y}(k)$, the transformation from orbital to band basis is not a simple rotation. Nevertheless, it can be expressed through

$$\begin{pmatrix} e_{1/2} \\ \bar{e}_{1/2} \end{pmatrix} = e^{i\phi} \begin{pmatrix} e^{i\phi_1} \cos \varphi_{1/2, \theta} & e^{i\phi_2} \sin \varphi_{1/2, \theta} \\ -e^{-i\phi_2} \sin \varphi_{1/2, \theta} & e^{-i\phi_1} \cos \varphi_{1/2, \theta} \end{pmatrix} \begin{pmatrix} f_{1/2} \\ f_{31/32} \end{pmatrix}, \quad (\text{S6})$$

where $e_{1/2} = e_{1, \mathbf{k}, \sigma}, e_{2, \mathbf{k}, \sigma}$ and $\bar{e}_{1/2}$ are operators for band fermions near the electron pockets, and the functions $\varphi_{1/2, \theta}$ and $\phi_{1/2}$ depend on the system parameters and determine the relative spectral weight of xz/yz and xy orbitals. We set $e_{1/2}$ to describe the electrons in the band that crosses the Fermi level. The dispersion of these fermions is $\xi_{e_1} = k_x^2/(2m_{ex}) + k_y^2/(2m_{ey}) - \mu_e$, $\xi_{e_2} = k_x^2/(2m_{ey}) + k_y^2/(2m_{ex}) - \mu_e$. For simplicity we assume $m_{ex} = m_{ey} = m_e$, i.e., set $\xi_{e_1} = \xi_{e_2} = \xi_e$

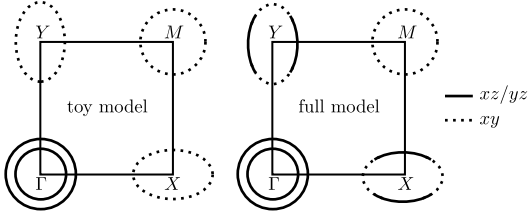


FIG. S1: The two 5-pocket models that we consider. The toy and the full model differ in the orbital content of electron pockets. For the full model, the electron pocket at X has contributions from d_{yz} and d_{xy} orbitals and the one at Y has contributions from d_{xz} and d_{xy} orbitals. For the toy model, we approximated these pockets as consisting exclusively of d_{xy} orbital.

$k^2/(2m_e) - \mu_e$. We checked that keeping m_{ex} and m_{ey} different will not change the pRG equations, once we properly rescale the couplings.

The electron propagator in orbital representation is expressed in terms of low energy fermions as

$$\begin{aligned}
G_{f_{1/2}, f_{1/2}}(i\omega, \mathbf{k}) &= G_{e1/e2}(i\omega, \mathbf{k}) \cos^2 \varphi_{1/2, \theta} \\
G_{f_{31/32}, f_{31/32}}(i\omega, \mathbf{k}) &= G_{e1/e2}(i\omega, \mathbf{k}) \sin^2 \varphi_{1/2, \theta} \\
G_{f_{1/2}, f_{31/32}}(i\omega, \mathbf{k}) &= G_{f_{31/32}, f_{1/2}}(i\omega, \mathbf{k})^* \\
&= G_{e1/e2}(i\omega, \mathbf{k}) e^{i(\phi_1 - \phi_2)} \cos \varphi_{1/2, \theta} \sin \varphi_{1/2, \theta},
\end{aligned} \tag{S7}$$

where $G_{e1/e2}(i\omega, \mathbf{k}) = (i\omega - \xi_e)^{-1}$ (k is counted from X in G_{e1} and from Y in G_{e2}).

B. The toy model

In the toy model, which we analyze in the main text prior to the full one, we approximate the orbital content of the two electron pockets as pure d_{xy} . In this case, the electron dispersions are already diagonal in the orbital basis, i.e. orbital and band representations are identical. Our notation for the electron operators is, in this approximation, $\psi_{X/Y, \mathbf{k}, \sigma} = f_{1/2, \mathbf{k}, \sigma}$, where 1/2 just labels the pockets. This toy model allows us to study the impact of the fifth pocket in a transparent way. Furthermore, we expect that the toy model already captures a substantial portion of the physics of the full model because adiabatically changing the tight-binding parameters of the underlying lattice model, one can move the spectral weight from d_{xz} (d_{yz}) to d_{xy} orbital everywhere on the electron pockets. There are, however, several features of the full model, which are not captured by the toy model. These are caused by the interactions which involve both xz/yz and xy -orbital states on the electron pockets.

C. Interactions

1. The toy model

As we said in the main text, the total number of different interactions between low-energy fermions in the toy model is 21. Of them 14 interactions involve fermions near the two Γ -centered hole pockets and the two electron pockets, and 7 involve fermions near the third hole pocket. In terms of the spinor components defined above, the 14 interaction terms are

$$\begin{aligned}
H_I^{4ps} &= U_1 \sum' \left[f_{1\sigma}^\dagger f_{1\sigma} d_{1\sigma'}^\dagger d_{1\sigma'} + f_{2\sigma}^\dagger f_{2\sigma} d_{2\sigma'}^\dagger d_{2\sigma'} \right] \\
&+ \bar{U}_1 \sum' \left[f_{2\sigma}^\dagger f_{2\sigma} d_{1\sigma'}^\dagger d_{1\sigma'} + f_{1\sigma}^\dagger f_{1\sigma} d_{2\sigma'}^\dagger d_{2\sigma'} \right] \\
&+ U_2 \sum' \left[f_{1\sigma}^\dagger d_{1\sigma} d_{1\sigma'}^\dagger f_{1\sigma'} + f_{2\sigma}^\dagger d_{2\sigma} d_{2\sigma'}^\dagger f_{2\sigma'} \right] \\
&+ \bar{U}_2 \sum' \left[f_{1\sigma}^\dagger d_{2\sigma} d_{2\sigma'}^\dagger f_{1\sigma'} + f_{2\sigma}^\dagger d_{1\sigma} d_{1\sigma'}^\dagger f_{2\sigma'} \right] \\
&+ \frac{U_3}{2} \sum' \left[f_{1\sigma}^\dagger d_{1\sigma} f_{1\sigma'}^\dagger d_{1\sigma'} + f_{2\sigma}^\dagger d_{2\sigma} f_{2\sigma'}^\dagger d_{2\sigma'} + h.c. \right] \\
&+ \frac{\bar{U}_3}{2} \sum' \left[f_{1\sigma}^\dagger d_{2\sigma} f_{1\sigma'}^\dagger d_{2\sigma'} + f_{2\sigma}^\dagger d_{1\sigma} f_{2\sigma'}^\dagger d_{1\sigma'} + h.c. \right] \\
&+ \frac{U_4}{2} \sum' \left[d_{1\sigma}^\dagger d_{1\sigma} d_{1\sigma'}^\dagger d_{1\sigma'} + d_{2\sigma}^\dagger d_{2\sigma} d_{2\sigma'}^\dagger d_{2\sigma'} \right] \\
&+ \frac{\bar{U}_4}{2} \sum' \left[d_{1\sigma}^\dagger d_{2\sigma} d_{1\sigma'}^\dagger d_{2\sigma'} + d_{2\sigma}^\dagger d_{1\sigma} d_{2\sigma'}^\dagger d_{1\sigma'} \right] \\
&+ \tilde{U}_4 \sum' d_{1\sigma}^\dagger d_{1\sigma} d_{2\sigma'}^\dagger d_{2\sigma'} + \tilde{\tilde{U}}_4 \sum' d_{1\sigma}^\dagger d_{2\sigma} d_{2\sigma'}^\dagger d_{1\sigma'} \\
&+ \frac{U_5}{2} \sum' \left[f_{1\sigma}^\dagger f_{1\sigma} f_{1\sigma'}^\dagger f_{1\sigma'} + f_{2\sigma}^\dagger f_{2\sigma} f_{2\sigma'}^\dagger f_{2\sigma'} \right] \\
&+ \frac{\bar{U}_5}{2} \sum' \left[f_{1\sigma}^\dagger f_{2\sigma} f_{1\sigma'}^\dagger f_{2\sigma'} + f_{2\sigma}^\dagger f_{1\sigma} f_{2\sigma'}^\dagger f_{1\sigma'} \right] \\
&+ \tilde{U}_5 \sum' f_{1\sigma}^\dagger f_{1\sigma} f_{2\sigma'}^\dagger f_{2\sigma'} + \tilde{\tilde{U}}_5 \sum' f_{1\sigma}^\dagger f_{2\sigma} f_{2\sigma'}^\dagger f_{1\sigma'},
\end{aligned} \tag{S8}$$

where the sum \sum' denotes the summation over spin σ, σ' , momenta $\mathbf{k}_1 + \mathbf{k}_2 - \mathbf{k}_3 - \mathbf{k}_4 = 0$ and includes the normalization factor $1/N$. The other 7 couplings are

$$\begin{aligned}
H_I^{5p} &= U_{1n} \sum' \left[d_{3\sigma}^\dagger d_{3\sigma} f_{1\sigma'}^\dagger f_{1\sigma'} + d_{3\sigma}^\dagger d_{3\sigma} f_{2\sigma'}^\dagger f_{2\sigma'} \right] \\
&+ U_{2n} \sum' \left[d_{3\sigma}^\dagger f_{1\sigma} f_{1\sigma'}^\dagger d_{3\sigma'} + d_{3\sigma}^\dagger f_{2\sigma} f_{2\sigma'}^\dagger d_{3\sigma'} \right] \\
&+ \frac{U_{3n}}{2} \sum' \left[d_{3\sigma}^\dagger f_{1\sigma} d_{3\sigma'}^\dagger f_{1\sigma'} + d_{3\sigma}^\dagger f_{2\sigma} d_{3\sigma'}^\dagger f_{2\sigma'} + h.c. \right] \\
&+ \frac{U_{4n}}{2} \sum' d_{3\sigma}^\dagger d_{3\sigma} d_{3\sigma'}^\dagger d_{3\sigma'} \\
&+ U_a \sum' \left[d_{3\sigma}^\dagger d_{3\sigma} d_{1\sigma'}^\dagger d_{1\sigma'} + d_{3\sigma}^\dagger d_{3\sigma} d_{2\sigma'}^\dagger d_{2\sigma'} \right] \\
&+ U_b \sum' \left[d_{3\sigma}^\dagger d_{1\sigma} d_{1\sigma'}^\dagger d_{3\sigma'} + d_{3\sigma}^\dagger d_{2\sigma} d_{2\sigma'}^\dagger d_{3\sigma'} \right] \\
&+ \frac{U_c}{2} \sum' \left[d_{3\sigma}^\dagger d_{1\sigma} d_{3\sigma'}^\dagger d_{1\sigma'} + d_{3\sigma}^\dagger d_{2\sigma} d_{3\sigma'}^\dagger d_{2\sigma'} + h.c. \right]
\end{aligned} \tag{S9}$$

The interactions of the toy model are sketched in Fig. S2. Each single interaction term in Eq. (S8) and Eq. (S9)

obeys the C_4 symmetry separately, which is why they do not need to flow equally under RG.

The bare values of the 21 couplings are expressed in terms of the parameters of the microscopic model for intra-orbital and inter-orbital interactions between fermions. The commonly used model approximates all interactions as local in real space:

$$\begin{aligned}
H_I = & U \sum_{i,\mu} n_{i,\mu,\uparrow} n_{i,\mu,\downarrow} + \frac{U'}{2} \sum_{i,\mu \neq \mu'} n_{i,\mu} n_{i,\mu'} \\
& + \frac{J}{2} \sum_{i,\mu \neq \mu'} \sum_{\sigma,\sigma'} d_{i,\mu,\sigma}^\dagger d_{i,\mu',\sigma'}^\dagger d_{i,\mu',\sigma'} d_{i,\mu,\sigma} \quad (\text{S10}) \\
& + \frac{J'}{2} \sum_{i,\mu \neq \mu'} \sum_{\sigma,\sigma'} d_{i,\mu,\sigma}^\dagger d_{i,\mu,\sigma'}^\dagger d_{i,\mu',\sigma'} d_{i,\mu',\sigma}.
\end{aligned}$$

Here the sums run over the sites i , the spin components σ , and the three orbitals $\mu = xy, xz, yz$. The density operator on site i in orbital μ is labeled by $n_{i,\mu} = \sum_{\sigma} n_{i,\mu,\sigma}$ and $n_{i,\mu,\sigma} = d_{i,\mu,\sigma}^\dagger d_{i,\mu,\sigma}$. The interactions in Eq. (S10) involve the Hubbard interaction U between electrons on the same orbital, the onsite repulsion U' between electrons in different orbitals, the Hund's rule coupling J and the pair-hopping term J' .

By comparing with Eq. (S10), we obtain the bare values of the 21 couplings

$$\begin{aligned}
U = U_4 = U_5 = \bar{U}_5 = \tilde{U}_5 = \tilde{\tilde{U}}_5 = U_{1n} = U_{2n} = U_{3n} = U_{4n} \\
U' = U_1 = \bar{U}_1 = \tilde{U}_4 = U_a \\
J = U_2 = \bar{U}_2 = \tilde{U}_4 = U_b \\
J' = U_3 = \bar{U}_3 = \tilde{U}_4 = U_c \quad (\text{S11})
\end{aligned}$$

Like we said in the main text, the 21 interactions all flow to different values under pRG. This implies that the system self-generates longer-ranged interactions as one progressively integrates out fermions with higher energies.

2. The full model

In the full model with d_{xz}/d_{xy} and d_{yz}/d_{xy} orbital content of fermions near the electron pockets, 23 more couplings are allowed by symmetry, what increases the total number of the C_4 -symmetric interaction terms to 44. 40 interactions involve pairs of fermions, with each pair near either Γ , X , Y , or M point. The 4 additional interactions involve fermions one near each of these points. Of the 23 new couplings, 13 are obtained by substituting f_1 and f_2 by f_{31} and f_{32} in Eqs. (S8) and (S9):

$$\begin{aligned}
H_I^{(1)} = & V_1 \sum' \left[f_{31\sigma}^\dagger f_{31\sigma} d_{1\sigma'}^\dagger d_{1\sigma'} + f_{32\sigma}^\dagger f_{32\sigma} d_{2\sigma'}^\dagger d_{2\sigma'} \right] \\
& + \bar{V}_1 \sum' \left[f_{32\sigma}^\dagger f_{32\sigma} d_{1\sigma'}^\dagger d_{1\sigma'} + f_{31\sigma}^\dagger f_{31\sigma} d_{2\sigma'}^\dagger d_{2\sigma'} \right] \\
& + V_2 \sum' \left[f_{31\sigma}^\dagger d_{1\sigma} d_{1\sigma'}^\dagger f_{31\sigma'} + f_{32\sigma}^\dagger d_{2\sigma} d_{2\sigma'}^\dagger f_{32\sigma'} \right]
\end{aligned}$$

$$\begin{aligned}
& + \bar{V}_2 \sum' \left[f_{31\sigma}^\dagger d_{2\sigma} d_{2\sigma'}^\dagger f_{31\sigma'} + f_{32\sigma}^\dagger d_{1\sigma} d_{1\sigma'}^\dagger f_{32\sigma'} \right] \\
& + \frac{V_3}{2} \sum' \left[f_{31\sigma}^\dagger d_{1\sigma} f_{31\sigma'}^\dagger d_{1\sigma'} + f_{32\sigma}^\dagger d_{2\sigma} f_{32\sigma'}^\dagger d_{2\sigma'} + h.c. \right] \\
& + \frac{\bar{V}_3}{2} \sum' \left[f_{31\sigma}^\dagger d_{2\sigma} f_{31\sigma'}^\dagger d_{2\sigma'} + f_{32\sigma}^\dagger d_{1\sigma} f_{32\sigma'}^\dagger d_{1\sigma'} + h.c. \right] \\
& + \frac{V_5}{2} \sum' \left[f_{31\sigma}^\dagger f_{31\sigma} f_{31\sigma'}^\dagger f_{31\sigma'} + f_{32\sigma}^\dagger f_{32\sigma} f_{32\sigma'}^\dagger f_{32\sigma'} \right] \\
& + \frac{\bar{V}_5}{2} \sum' \left[f_{31\sigma}^\dagger f_{32\sigma} f_{31\sigma'}^\dagger f_{32\sigma'} + f_{32\sigma}^\dagger f_{31\sigma} f_{32\sigma'}^\dagger f_{31\sigma'} \right] \\
& + \tilde{V}_5 \sum' f_{31\sigma}^\dagger f_{31\sigma} f_{32\sigma'}^\dagger f_{32\sigma'} + \tilde{\tilde{V}}_5 \sum' f_{31\sigma}^\dagger f_{32\sigma} f_{32\sigma'}^\dagger f_{31\sigma'} \\
& + V_{1n} \sum' \left[d_{3\sigma}^\dagger d_{3\sigma} f_{31\sigma'}^\dagger f_{31\sigma'} + d_{3\sigma}^\dagger d_{3\sigma} f_{32\sigma'}^\dagger f_{32\sigma'} \right] \\
& + V_{2n} \sum' \left[d_{3\sigma}^\dagger f_{31\sigma} f_{31\sigma'}^\dagger d_{3\sigma'} + d_{3\sigma}^\dagger f_{32\sigma} f_{32\sigma'}^\dagger d_{3\sigma'} \right] \\
& + \frac{V_{3n}}{2} \sum' \left[d_{3\sigma}^\dagger f_{31\sigma} d_{3\sigma'}^\dagger f_{31\sigma'} + d_{3\sigma}^\dagger f_{32\sigma} d_{3\sigma'}^\dagger f_{32\sigma'} + h.c. \right] \quad (\text{S12})
\end{aligned}$$

Further six couplings come from interactions involving xy and xz/yz orbital states on the electron pockets

$$\begin{aligned}
H_I^{(2)} = & V_a \sum' \left[f_{31\sigma}^\dagger f_{31\sigma} f_{1\sigma'}^\dagger f_{1\sigma'} + f_{32\sigma}^\dagger f_{32\sigma} f_{2\sigma'}^\dagger f_{2\sigma'} \right] \\
& + \bar{V}_a \sum' \left[f_{32\sigma}^\dagger f_{32\sigma} f_{1\sigma'}^\dagger f_{1\sigma'} + f_{31\sigma}^\dagger f_{31\sigma} f_{2\sigma'}^\dagger f_{2\sigma'} \right] \\
& + V_b \sum' \left[f_{31\sigma}^\dagger f_{1\sigma} f_{1\sigma'}^\dagger f_{31\sigma'} + f_{32\sigma}^\dagger f_{2\sigma} f_{2\sigma'}^\dagger f_{32\sigma'} \right] \\
& + \bar{V}_b \sum' \left[f_{31\sigma}^\dagger f_{2\sigma} f_{2\sigma'}^\dagger f_{31\sigma'} + f_{32\sigma}^\dagger f_{1\sigma} f_{1\sigma'}^\dagger f_{32\sigma'} \right] \\
& + \frac{V_c}{2} \sum' \left[f_{31\sigma}^\dagger f_{1\sigma} f_{31\sigma'}^\dagger f_{1\sigma'} + f_{32\sigma}^\dagger f_{2\sigma} f_{32\sigma'}^\dagger f_{2\sigma'} + h.c. \right] \\
& + \frac{\bar{V}_c}{2} \sum' \left[f_{31\sigma}^\dagger f_{2\sigma} f_{31\sigma'}^\dagger f_{2\sigma'} + f_{32\sigma}^\dagger f_{1\sigma} f_{32\sigma'}^\dagger f_{1\sigma'} + h.c. \right] \quad (\text{S13})
\end{aligned}$$

We show these interactions graphically in Fig. S3. Note that, in contrast to the simplified model, $f_{1/2}$ now labels fermions with yz/xz orbital content, whereas $f_{31,32}$ labels fermions with xy orbital content.

Finally there are four additional interactions that, in contrast to the previous 40 interactions, involve fermions near each of the four high-symmetry points Γ , X , Y , M . In explicit form, these interactions are

$$\begin{aligned}
H_I^{(3)} = & W_1 \sum' \left[f_{1\sigma}^\dagger d_{3\sigma} f_{32\sigma'}^\dagger d_{1\sigma'} + f_{2\sigma}^\dagger d_{3\sigma} f_{31\sigma'}^\dagger d_{2\sigma'} + h.c. \right] \\
& + W_2 \sum' \left[f_{31\sigma}^\dagger d_{3\sigma} f_{2\sigma'}^\dagger d_{2\sigma'} + f_{32\sigma}^\dagger d_{3\sigma} f_{1\sigma'}^\dagger d_{1\sigma'} + h.c. \right] \\
& + W_3 \sum' \left[f_{1\sigma}^\dagger d_{1\sigma} d_{3\sigma'}^\dagger f_{32\sigma'} + f_{2\sigma}^\dagger d_{2\sigma} d_{3\sigma'}^\dagger f_{31\sigma'} + h.c. \right] \\
& + W_4 \sum' \left[f_{31\sigma}^\dagger d_{2\sigma} d_{3\sigma'}^\dagger f_{2\sigma'} + f_{32\sigma}^\dagger d_{1\sigma} d_{3\sigma'}^\dagger f_{1\sigma'} + h.c. \right] \quad (\text{S14})
\end{aligned}$$

We checked explicitly that these four additional interactions do not affect the behavior near each of the four stable fixed trajectories, which we obtained by solving the pRG equations for 40 couplings (see Sec. II B). This

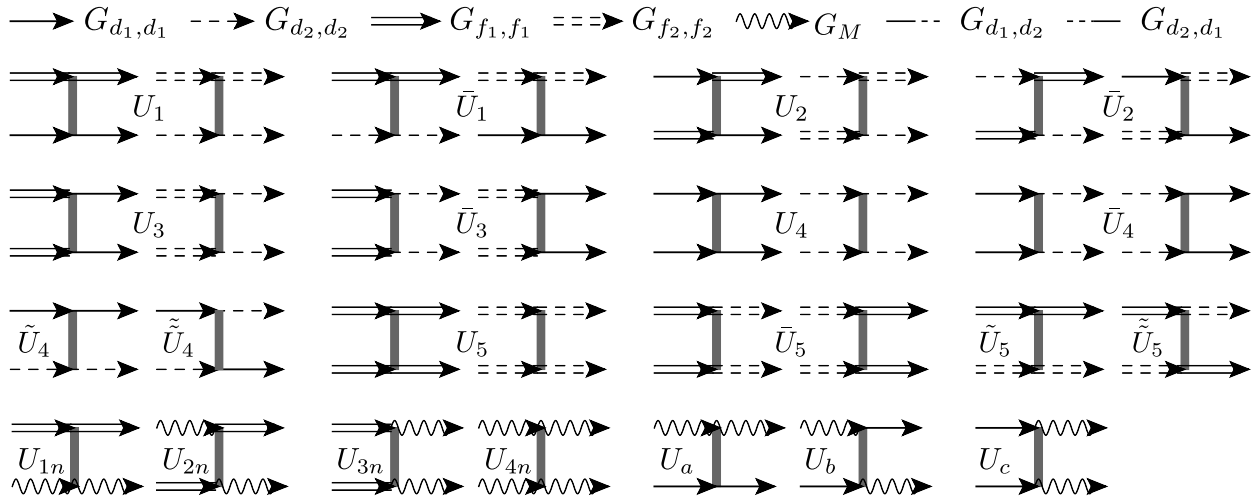


FIG. S2: Diagrammatic representation of the 21 interaction terms in the toy model. Each interaction term is invariant under C_4 rotation.

is what we presented in the main text. We also verified that these additional interactions do not generate new fixed trajectories, if the bare values of these interactions are within certain limits. Outside these limits, the 4 additional interactions may, in principle, move the system towards a new stable fixed trajectory. We did not explore this possibility here and in the following we neglect these four additional interactions.

Like we did for the toy model, we express the bare values of the 40 couplings in terms of U, U', J, J' . We have

$$\begin{aligned}
 U &= U_1 = U_2 = U_3 = U_4 = U_5 = \bar{U}_5 = U_{4n} = V_5 = \bar{V}_5 \\
 &= \tilde{V}_5 = \tilde{\tilde{V}}_5 = V_{1n} = V_{2n} = V_{3n} \\
 U' &= \bar{U}_1 = \tilde{U}_4 = \tilde{\tilde{U}}_5 = U_{1n} = U_a = V_a = \bar{V}_a = V_1 = \bar{V}_1 \\
 J &= \bar{U}_2 = \tilde{\tilde{U}}_4 = \tilde{\tilde{\tilde{U}}}_5 = U_{2n} = U_b = V_b = \bar{V}_b = V_2 = \bar{V}_2 \\
 J' &= \bar{U}_3 = \bar{U}_4 = \bar{U}_5 = U_{3n} = U_c = V_c = \bar{V}_c = V_3 = \bar{V}_3.
 \end{aligned}
 \tag{S15}$$

II. ANALYTIC PARGUET RG FOR 5-POCKET MODEL

We employ a pRG approach to study the hierarchy of the orders that the system develops at low energies. The pRG procedure allows us to see how the susceptibilities in different ordering channels evolve as the system flows to low energies, including their mutual feedback. In the pRG procedure, one integrates out fermions with energies down to a progressively smaller running energy E and observes how the couplings vary as E gets smaller. We describe this flow of interactions in terms of the RG scale $L = \log \Lambda/E$, where Λ is the UV-cut-off, generally of the order of the bandwidth. The logarithmic energy scale L appears due to the fact that the polarization bubbles in the particle-particle channel at zero total momen-

tum *and* the particle-hole channel at momenta $(\pi, 0)$ and $(0, \pi)$ are logarithmical. As a result of the integration procedure, we obtain coupled differential equations -the flow equations- for all the interactions, describing their evolution with L . We solve for the running couplings $U_i(L)$ and use these solutions as inputs to calculate susceptibilities in different ordering channels (SDW, CDW, superconducting and Pomeranchuk channels). An instability in a particular channel is signaled by the divergence of the corresponding susceptibility at a scale L_{cr} . Below we show the details of pRG analysis for the toy model and the full model. We recall that pRG analysis works when E is larger than the Fermi energy, i.e., when $L < L_F = \log \Lambda/E_F$ (see, e.g., Ref. [?]). If $L_{cr} < L_F$, the pRG analysis works all the way to the leading instability. If $L_{cr} > L_F$, pRG analysis allows one to determine the largest susceptibility at $L = L_F$. It is likely (although not guaranteed) that this susceptibility will diverge first at a lower energy.

A. PRG for the toy model

1. PRG equations and fixed trajectories

We derive the pRG equations by collecting all possible one-loop diagrams that contribute to logarithmic renormalization of each of the interactions. The procedure has been described Ref. [S4] (for a simplified 4-pocket, two-orbital model) and in Ref. [?] for 3-pocket, one-orbital model. We follow the same line of reasoning as in these works. We obtain the pRG equations for our 5-pocket model by combining and modifying pRG equations from these two models.

Like in Ref. [S4] we find that pRG equations for 6 combinations of the couplings $(\tilde{U}_4 \pm \tilde{\tilde{U}}_4)$, $(\tilde{U}_5 \pm \tilde{\tilde{U}}_5)$ and $(\tilde{U}_a \pm \tilde{\tilde{U}}_b)$ decouple from other RG equations, and these

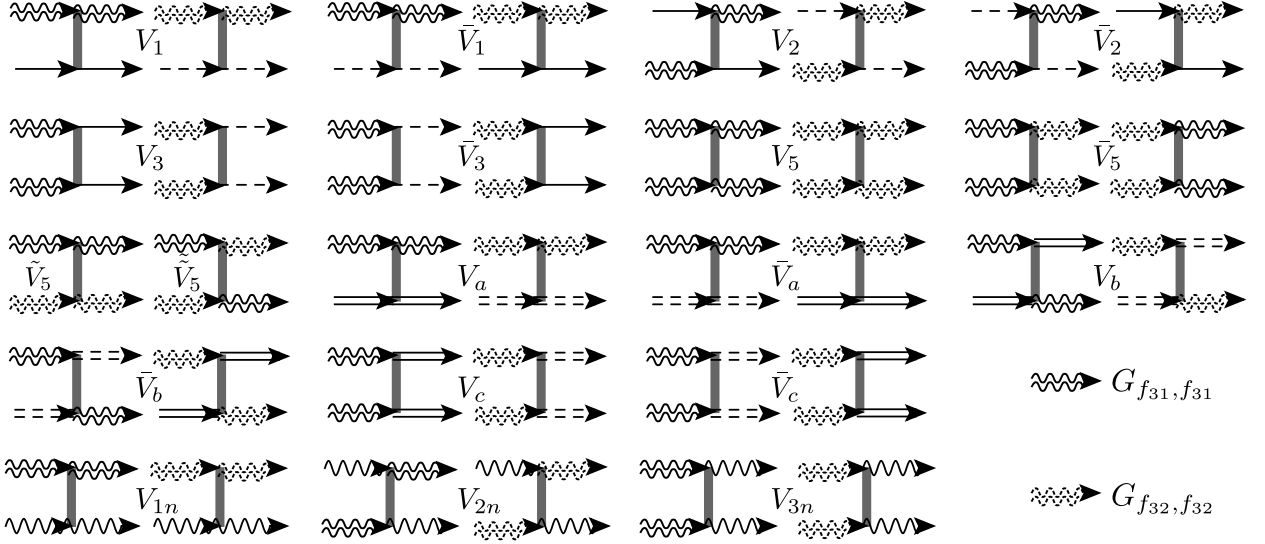


FIG. S3: Additional interactions allowed by C_4 symmetry in the full model.

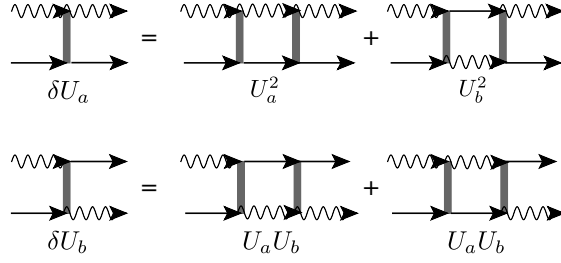


FIG. S4: Diagrammatic representation of the 1-loop renormalizations of the interactions U_a and U_b . They decouple from the remaining interactions and are representative for the subgroup of interactions flowing to zero.

combinations all flow to zero if their bare values are positive, which is the case for $U' \geq J$. We assume that this inequality holds. If it does not hold, the system may develop a superconducting instability in the spin-triplet A_{2g} channel (Ref. [S35]). Representative diagrams for the renormalizations of the couplings from this group of 6 are shown in Fig. S4. The 6 pRG equations are:

$$\begin{aligned}
 4\pi \frac{d}{dL} (\tilde{U}_4 \pm \tilde{\tilde{U}}_4) &= -c_{pp}^{(1)} (\tilde{U}_4 \pm \tilde{\tilde{U}}_4)^2 \\
 4\pi \frac{d}{dL} (\tilde{U}_5 \pm \tilde{\tilde{U}}_5) &= -c_{pp}^{(2)} (\tilde{U}_5 \pm \tilde{\tilde{U}}_5)^2 \\
 4\pi \frac{d}{dL} (U_a \pm U_b) &= -c_{pp}^{(3)} (U_a \pm U_b)^2,
 \end{aligned} \tag{S16}$$

where $c_{pp}^{(1)} = \frac{1}{8}(m_c + m_d + 12 \frac{m_c m_d}{m_c + m_d} \pm \frac{(m_c - m_d)^2}{m_c + m_d})$, $c_{pp}^{(2)} = m_e$ and $c_{pp}^{(3)} = \frac{m_M m_c}{m_M + m_c} + \frac{m_M m_d}{m_M + m_d}$. The pRG equations for the other remaining 15 couplings are

$$4\pi \frac{d}{dL} U_1 = A(U_1^2 + U_3^2)$$

$$4\pi \frac{d}{dL} \bar{U}_1 = A(\bar{U}_1^2 + \bar{U}_3^2)$$

$$4\pi \frac{d}{dL} U_{1n} = A_n(U_{1n}^2 + U_{3n}^2)$$

$$4\pi \frac{d}{dL} U_2 = 2AU_2(U_1 - U_2)$$

$$4\pi \frac{d}{dL} \bar{U}_2 = 2A\bar{U}_2(\bar{U}_1 - \bar{U}_2)$$

$$4\pi \frac{d}{dL} U_{2n} = 2A_n U_{2n}(U_{1n} - U_{2n})$$

$$\begin{aligned}
 4\pi \frac{d}{dL} U_3 &= 2AU_3(2U_1 - U_2) - A_e(U_3U_5 + \bar{U}_3\bar{U}_5) \\
 &\quad - A_h(U_3U_4 + \bar{U}_3\bar{U}_4) - A_h^-(U_3\bar{U}_4 + \bar{U}_3U_4) - A_M U_{3n} U_c
 \end{aligned}$$

$$\begin{aligned}
 4\pi \frac{d}{dL} \bar{U}_3 &= 2A\bar{U}_3(2\bar{U}_1 - \bar{U}_2) - A_e(\bar{U}_3U_5 + U_3\bar{U}_5) \\
 &\quad - A_h(\bar{U}_3U_4 + U_3\bar{U}_4) - A_h^-(U_3U_4 + \bar{U}_3\bar{U}_4) - A_M U_{3n} U_c
 \end{aligned}$$

$$\begin{aligned}
 4\pi \frac{d}{dL} U_{3n} &= 2A_n U_{3n}(2U_{1n} - U_{2n}) - A_e U_{3n}(U_5 + \bar{U}_5) \\
 &\quad - A_M U_{3n} U_{4n} - (A_h + A_h^-)(U_3 + \bar{U}_3) U_c
 \end{aligned}$$

$$\begin{aligned}
 4\pi \frac{d}{dL} U_4 &= -A_h(U_4^2 + \bar{U}_4^2) - 2A_h^-(U_4\bar{U}_4) - A_e(U_3^2 + \bar{U}_3^2) \\
 &\quad - A_M U_c^2
 \end{aligned}$$

$$\begin{aligned}
 4\pi \frac{d}{dL} \bar{U}_4 &= -2A_h U_4 \bar{U}_4 - A_h^-(U_4^2 + \bar{U}_4^2) - 2A_e U_3 \bar{U}_3 \\
 &\quad - A_M U_c^2
 \end{aligned}$$

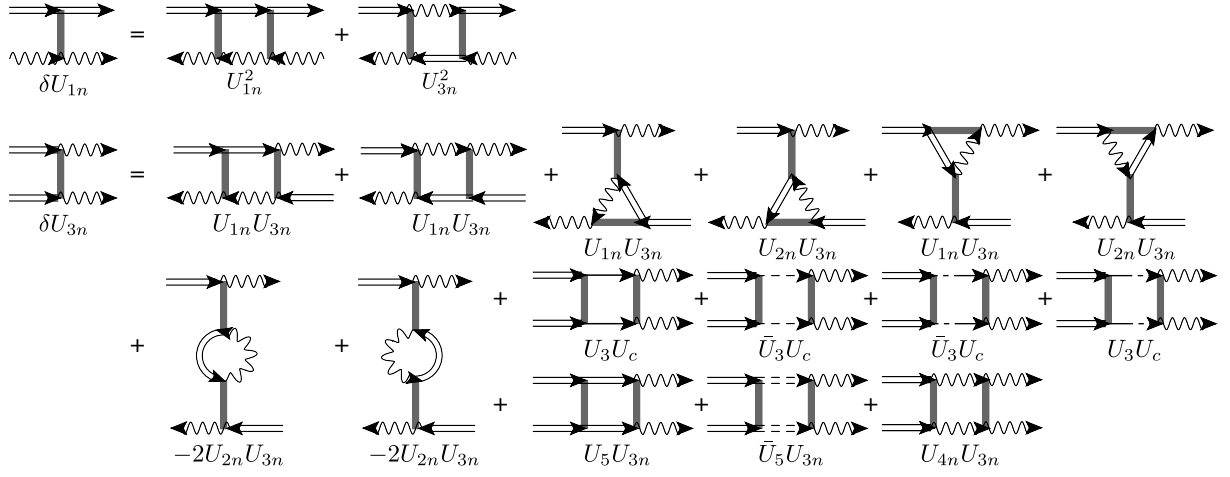


FIG. S5: Diagrammatic representation of the 1-loop renormalization of the interactions U_{1n} and U_{3n} .

$$\begin{aligned}
4\pi \frac{d}{dL} U_{4n} &= -A_M U_{4n}^2 - 2A_e U_{3n}^2 - 2(A_h + A_h^-) U_c^2 \\
4\pi \frac{d}{dL} U_5 &= -A_e (U_5^2 + \bar{U}_5^2) - A_h (U_3^2 + \bar{U}_3^2) - 2A_h^- U_3 \bar{U}_3 \\
&\quad - A_M U_{3n}^2 \\
4\pi \frac{d}{dL} \bar{U}_5 &= -2A_e U_5 \bar{U}_5 - 2A_h U_3 \bar{U}_3 - A_h^- (U_3^2 + \bar{U}_3^2) \\
&\quad - A_M U_{3n}^2 \\
4\pi \frac{d}{dL} U_c &= -(A_h + A_h^-) (U_4 + \bar{U}_4) U_c - A_M U_{4n} U_c \\
&\quad - A_3 (U_3 + \bar{U}_3) U_{3n}. \tag{S17}
\end{aligned}$$

As an example, the one-loop diagrams that renormalize U_{1n} and U_{3n} are presented in Fig. S5. The numerical prefactors in the r.h.s. of pRG equations are $A = \frac{m_e m_c}{m_e + m_c} + \frac{m_e m_d}{m_e + m_d}$, $A_n = \frac{m_M m_e}{m_M + m_e}$, $A_e = m_e$, $A_h = \frac{3}{8}(m_c + m_d) + \frac{1}{2} \frac{m_e m_d}{m_c + m_d}$, $A_h^- = \frac{1}{8} \frac{(m_c - m_d)^2}{m_c + m_d}$ and $A_M = m_M$. Note that the contribution $A_h^- = (m_c - m_d)^2 / (8(m_c + m_d))$ comes from the G_{d_1, d_2} the propagator for fermions near the Γ -centered hole pockets (see Eq.(S5)).

To proceed, we note that, if $U_i = \bar{U}_i$, then $d_L U_i = d_L \bar{U}_i$. We have checked that the trajectory with this property is a stable one. We searched for other potential stable fixed trajectories, but did not find one. Hence we set $U_i = \bar{U}_i$. We further introduce the dimensionless couplings $u_{1,2} = A/(4\pi)U_{1,2}$, $u_3 = A/(4\pi)aU_3$, $u_4 = A_h/(4\pi)U_4$, $u_5 = A_e/(4\pi)U_5$, $u_{1n,2n} = A_n/(4\pi)U_{1n,2n}$, $u_{3n} = A_n/(4\pi)a_n U_{3n}$, $u_{4n} = A_M/(4\pi)U_{4n}$ and $u_{5n} = \sqrt{A_M A_h}/(4\pi)U_c$ and define $a = \sqrt{A_h A_e}/A$ and $a_n = \sqrt{A_M A_e}/A_n$ and $b = 1 + A_h^-/A_h$. Then we obtain the pRG equations

$$\begin{aligned}
\dot{u}_1 &= u_1^2 + \frac{u_3^2}{a^2} \\
\dot{u}_{1n} &= u_{1n}^2 + \frac{u_{3n}^2}{a_n^2} \\
\dot{u}_2 &= 2u_2(u_1 - u_2)
\end{aligned} \tag{S18}$$

$$\begin{aligned}
\dot{u}_{2n} &= 2u_{2n}(u_{1n} - u_{2n}) \\
\dot{u}_3 &= 2u_3(2u_1 - u_2 - u_5) - 2bu_3u_4 - u_{3n}u_{5n} \\
\dot{u}_{3n} &= 2u_{3n}(2u_{1n} - u_{2n} - u_5) - u_{3n}u_{4n} - 2bu_3u_{5n} \\
\dot{u}_4 &= -2bu_4^2 - 2u_3^2 - 2u_{5n}^2 \\
\dot{u}_{4n} &= -u_{4n}^2 - 2u_{3n}^2 - 2bu_{5n}^2 \\
\dot{u}_5 &= -2u_5^2 - 2bu_3^2 - u_{3n}^2 \\
\dot{u}_{5n} &= -2bu_4u_{5n} - u_{4n}u_{5n} - 2u_3u_{3n},
\end{aligned}$$

which we presented in the main text for $a = a_n = b = 1$.

2. The solution of PRG equations

To simplify the analysis we assume $m_c \approx m_d$ and neglect the contribution from A_h^- , i.e. set $A_h^- = 0$. We searched for different fixed trajectories of Eq. (S17) along which the couplings diverge, but their ratios tend to fixed values. This can be seen in Fig. S6. Accordingly, we single out one of the coupling, say u_0 , and write all other couplings as

$$u_i = \gamma_i u_0, \tag{S19}$$

Along the fixed trajectory, u_0 flows to infinity, but γ_i tend to finite values. Solving for the fixed trajectory of the set of coupled pRG equations, Eq. (S17), then reduces to finding the fixed point solution of

$$\beta_i := \partial_L \gamma_i = \frac{1}{u_i} (\partial_L u_i - \gamma_i \partial_L u_0) = 0. \tag{S20}$$

The fixed trajectory is stable if small perturbations around the fixed point do not grow, i.e. the stability matrix $\partial \beta_i / \partial \gamma_j |_{\gamma^*}$, which describes the linearized flow around the fixed point, should have only negative eigenvalues. For the toy model we find two stable fixed trajectories, separated by a fixed point solution with a single unstable direction. In the main text we labeled the two

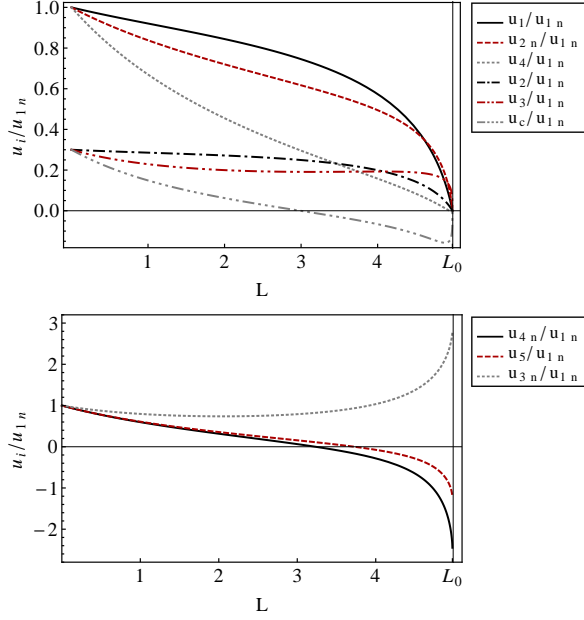


FIG. S6: Ratios of couplings for the flow to the 3-pocket fixed trajectory (3p) in the toy model for bare values $U = U' = 0.1/N_F$, $J = J' = 0.03/N_F$ and $a = a_n = 1$, N_F is the density of states on the FSs. All ratios tend to zero (upper penal), except for those within the triad of electron pockets and the M -centered hole pocket.

stable fixed trajectories as effective 4-pocket model (4p) and effective 3-pocket mode (3p). The behavior of the couplings along these two stable fixed trajectories is

(1) 4p

$$\begin{aligned}
 u_i &= \gamma_i u_1 \\
 u_1 &= \frac{1}{1 + \gamma_3^2/a^2} \frac{1}{L_0 - L} \\
 \gamma_2 = \gamma_{1n} = \gamma_{2n} = \gamma_{3n} = \gamma_{4n} = \gamma_c &= 0 \\
 \gamma_3 &= \pm a \sqrt{8a^2 - 1 + 4\sqrt{1 - a^2 + 4a^4}} \\
 \gamma_4 = \gamma_5 &= 1 - 2a^2 - \sqrt{1 - a^2 + 4a^4} \quad (S21)
 \end{aligned}$$

(2) 3p

$$\begin{aligned}
 u_i &= \gamma_i u_{1n} \\
 u_{1n} &= \frac{1}{1 + \gamma_{3n}^2/a_n^2} \frac{1}{L_0 - L} \\
 \gamma_{2n} = \gamma_c = \gamma_1 = \gamma_2 = \gamma_3 = \gamma_4 &= 0 \\
 \gamma_{3n} &= \pm a_n \sqrt{4a_n^2 - 1 + 2\sqrt{4 - 2a_n^2 + 4a_n^4}} \\
 \gamma_{4n} = 2\gamma_5 &= 2 - 2a_n^2 - \sqrt{4 - 2a_n^2 + 4a_n^4} \quad (S22)
 \end{aligned}$$

Because the bare values for γ_3 , γ_{3n} are positive, the system reaches the stable FT with positive γ_3 , γ_{3n} . We see that along the stable fixed trajectories, either all γ_i for interactions with the Γ -centered hole pockets vanish (3p),

or all γ_i for the interactions with the third hole pocket at M vanish (4p). This does not mean that the interactions themselves vanish, it only means that these interactions do not grow as fast as other interactions. These couplings actually still increase under pRG but with exponents smaller than one. This means that, to leading order, the system flows to either 4-pocket model (4p) or 3-pocket model (3p). However the subleading terms still have an impact on the emergent order, as they determine how the order parameter behaves at the remaining hole pocket(s).

The third, weakly unstable fixed trajectory is symmetry-enhanced in the sense that $u_1 = u_{1n}$, and $u_3/a = u_{3n}/a_n$. Along this trajectory all ratios (except for γ_2, γ_{2n}) attain finite values. Specifically, we obtain

$$\begin{aligned}
 u_i &= \gamma_i u_1 \\
 u_1 &= \frac{1}{1 + \gamma_3^2/a^2} \frac{1}{L_0 - L} \\
 \gamma_{1n} = \gamma_1 &= 1 \quad \frac{\gamma_{3n}}{a_n} = \pm \frac{\gamma_3}{a} \quad \gamma_2 = \gamma_{2n} = 0 \\
 \gamma_3 &= \sqrt{8a^4 - a^2 + 4a^2 a_n^2 + a^2 \sqrt{15 + (8a^2 + 4a_n^2 - 1)^2}} \\
 \gamma_5 &= 1 - a_n^2 - 2a^2 - \sqrt{1 + a_n^4 - a^2 + 4a^4 + a_n^2(4a^2 - 1)} \\
 \gamma_c &= \pm a_n \frac{2a - \sqrt{2\gamma_3^2 a_n^2 + 4a^2(1 + \gamma_3^2)}}{a_n^2 + 2a^2} \\
 \gamma_4 &= \pm \frac{a_n}{2a} \gamma_c + \frac{\gamma_3^2}{4a^2} - \frac{3}{4} \\
 \gamma_{4n} &= \mp \frac{2a}{a_n} \gamma_c + \gamma_5 \quad (S23)
 \end{aligned}$$

For $a = a_n = 1$ γ_i in (S23) reduce to

$$\begin{aligned}
 \gamma_3 &= \pm \gamma_{3n} \quad \gamma_4 = \gamma_{4n} = \pm \gamma_c \\
 \gamma_3 &= \sqrt{11 + 2\sqrt{34}} \quad \gamma_4 = -\frac{1}{3}(4 + \sqrt{34}) \\
 \gamma_5 &= -2 - \sqrt{\frac{17}{2}} \quad (S24)
 \end{aligned}$$

Like we said, this fixed trajectory has one unstable direction when we consider deviations from it. We verified that, depending on the sign of deviation along the unstable direction, the system flows either to one or to the other stable fixed trajectory. We present the phase diagram for different bare values in the main text and here present the result of our study of the stability regimes of 4p and 3p at various a_n/a in Fig.S7.

3. Susceptibilities

To decide which order wins and develops at low energies, we introduce vertices Γ_i that describe the coupling between fermions and order parameters. The vertices in turn determine the susceptibilities in the corresponding ordering channel, whose divergence would signal a

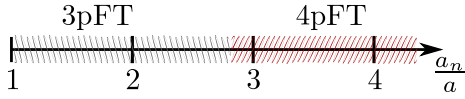


FIG. S7: Fixed trajectory at the end of the flow for different values of a_n/a . 3pFT (4pFT) denotes the effective 3p (4p) model. Bare values are $U = U'$, $J = J'$ and $J/U = 0.3$.

phase transition. Here we focus on SDW, CDW, and SC channels. The analysis of the susceptibilities in the Pomeranchuk channels is discussed afterwards.

The vertices are renormalized by the corresponding polarization bubbles and diverge with a certain exponent when the running couplings approach the fixed trajectory, as $\Gamma_i \propto (L_0 - L)^{-\beta}$. The susceptibilities

$$\chi_i - \chi_0 \propto \int_L dL' \Gamma_i^2(L'), \quad (\text{S25})$$

then behave as $\chi \propto (L_0 - L)^{1-2\beta} + \text{const.}$ In order to diverge the vertex exponent must satisfy $\beta \geq 1/2$. The one-loop renormalization of the vertices are shown in Fig. S8. In analytic form, the pRG equations for the vertices in the SDW and CDW channels are

$$\begin{aligned} \partial_L \Gamma_{SDW}^\Gamma &= \left(u_1 + \frac{u_3}{a}\right) \Gamma_{SDW}^\Gamma \\ \partial_L \Gamma_{SDW}^M &= \left(u_{1n} + \frac{u_{3n}}{a_n}\right) \Gamma_{SDW}^M \\ \partial_L \Gamma_{CDW}^\Gamma &= \left(u_1 - 2u_2 - \frac{u_3}{a}\right) \Gamma_{CDW}^\Gamma \\ \partial_L \Gamma_{CDW}^M &= \left(u_{1n} - 2u_{2n} - \frac{u_{3n}}{a_n}\right) \Gamma_{CDW}^M. \end{aligned} \quad (\text{S26})$$

By inserting the values for the fixed trajectories, we obtain the exponents β_i :

$$\begin{aligned} \beta_{SDW}^{(4p)} &= \frac{1 + \gamma_3/a}{1 + \gamma_3^2/a^2} & \beta_{CDW}^{(4p)} &= \frac{1 - \gamma_3/a}{1 + \gamma_3^2/a^2} \\ \beta_{SDW}^{(3p)} &= \frac{1 + \gamma_{3n}/a_n}{1 + \gamma_{3n}^2/a_n^2} & \beta_{CDW}^{(3p)} &= \frac{1 - \gamma_{3n}/a_n}{1 + \gamma_{3n}^2/a_n^2}. \end{aligned} \quad (\text{S27})$$

Note that γ_3, γ_{3n} also depend on a, a_n in these expressions. The exponents attain their maximal values at $a = 1, a_n = 1$ with $\beta_{SDW}^{(4p)} \approx 0.30$, $\beta_{CDW}^{(4p)} \approx -0.18$ and $\beta_{SDW}^{(3p)} \approx 0.43$, $\beta_{CDW}^{(3p)} \approx -0.20$. These values do not lead to a divergent susceptibility, i.e. the corresponding order does not develop if the normal state becomes unstable before the Fermi energy is reached.

The pRG flow of the vertices in the particle-particle channel obeys

$$\partial_L \begin{pmatrix} \Gamma_{SC}^e \\ \Gamma_{SC}^\Gamma \\ \Gamma_{SC}^M \end{pmatrix} = \begin{pmatrix} -2u_5 & -2u_3 & -2u_{3n} \\ -2u_3 & -2u_4 & -2u_c \\ -u_{3n} & -u_c & -u_{4n} \end{pmatrix} \begin{pmatrix} \Gamma_{SC}^e \\ \Gamma_{SC}^\Gamma \\ \Gamma_{SC}^M \end{pmatrix}, \quad (\text{S28})$$

where we have absorbed different prefactors into Γ_{SC} as $\sqrt{A_h/A_e} \Gamma_{SC}^\Gamma \rightarrow \Gamma_{SC}^\Gamma, \sqrt{A_M/A_e} \Gamma_{SC}^M \rightarrow \Gamma_{SC}^M$. For 4pFT

and 3pFT, this set reduces to a 2x2 matrix, and the diagonalization of Eq. (S28) yields in these two cases

$$\begin{aligned} \beta_{SC,+ - / + +}^{(4p)} &= \frac{-\gamma_4 - \gamma_5 \pm \sqrt{(\gamma_4 - \gamma_5)^2 + 4\gamma_3^2/a^2}}{1 + \gamma_3^2/a^2} \\ \beta_{SC,+ - / + +}^{(3p)} &= \frac{-\gamma_{4n} - 2\gamma_5 \pm \sqrt{(\gamma_{4n} - 2\gamma_5)^2 + 8\gamma_{3n}^2/a_n^2}}{1 + \gamma_{3n}^2/a_n^2}. \end{aligned} \quad (\text{S29})$$

The largest eigenvalues correspond to the s_{+-} superconducting state and satisfy $\beta_{SC,+ -} > 1/2$. For $a = a_n = 1$ they are $\beta_{SC,+ -}^{(4p)} = 0.86$, and $\beta_{SC,+ -}^{(3p)} = 0.72$. Because these β_{SC} are larger than $1/2$, we find that the system develops superconductivity at low energies rather than SDW or CDW order. From the analysis of the fixed trajectory we can infer that the gap changes sign either between the electron pockets and the two Γ -centered hole pockets (for 4p), or between the electron pockets and the M -centered hole pocket (for 3p). In both cases, this is conventional s^{+-} gap structure.

To determine the sign of the superconducting gap on the remaining hole pocket(s), we must include the residual interactions (the once which diverge with smaller exponents). To do this and to verify our analytical reasoning, we solved the set of pRG equations for the couplings and the set of the vertices in the SC channel, Eq. (S28), numerically. We find two positive (attractive) and one negative eigenvalue in the SC channel. The negative one obviously corresponds to repulsive interaction in s^{++} channel. The positive eigenvalues correspond to s^{+-} gap structure. For the largest positive eigenvalue along the 3p FT or 4p FT the gap(s) on the remaining hole pocket(s) align such that the sign of the gap on all three hole pockets is the same (and opposite to the gap sign on the two electron pockets). This is the "conventional" s^{+-} gap structure. However, the size of the vertex, which is related to the gap size, on the residual pocket is smaller than on the dominant pockets. The smaller positive eigenvalue along the 3p FT or the 4p FT actually starts negative at small L and then changes the sign in the process of the RG flow. For the 4p FT, the gap structure that corresponds to this eigenvalue has the same sign of the gap on the M -centered hole pocket as on the electron pockets, i.e., there is one sign of the gap on the two Γ -centered hole pockets and another sign on the other three pockets. For the 3p FT and for this eigenvalue, the sign of the gap on the Γ -centered hole pockets and on the electron pockets is the same, and opposite to that on the M -hole pocket. The gap structure of this kind was proposed in Ref. [S29] and termed as "orbital anti-phase". Our RG analysis shows that along the fixed trajectory such a state is subleading to a conventional s^{+-} . Finally, we computed the gap structure along the weakly unstable FT of Eq. (S23) and found that it is also a conventional s^{+-} . We do not find d-wave order.

To analyze orbital ordering, we calculate the vertices and susceptibilities in the Pomeranchuk channel with the orbital densities $n_\mu = d_\mu^\dagger d_\mu$ as order parameters. The

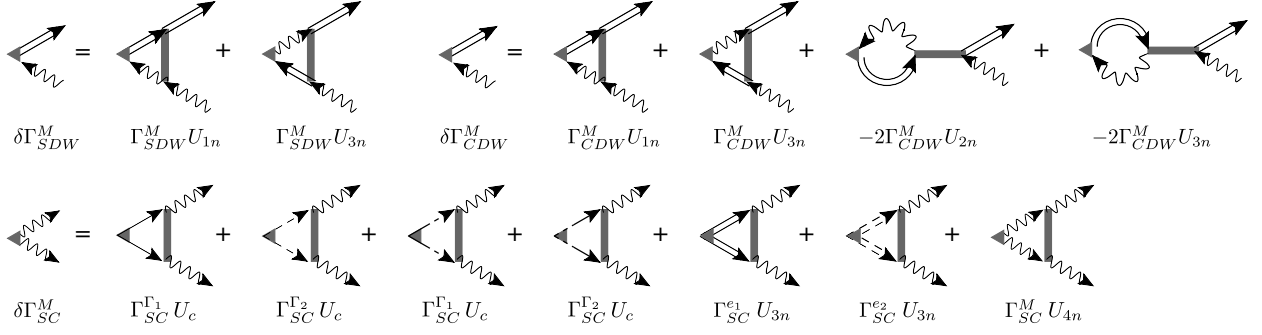


FIG. S8: Diagrammatic representation of the 1-loop renormalization of representative SDW, CDW, and SC vertices. In the RG equations of the superconducting vertices, only the combinations $\Gamma_{SC}^\Gamma := \Gamma_{SC}^{\Gamma_1} + \Gamma_{SC}^{\Gamma_2}$, $\Gamma_{SC}^e := \Gamma_{SC}^{e_1} + \Gamma_{SC}^{e_2}$ appear.

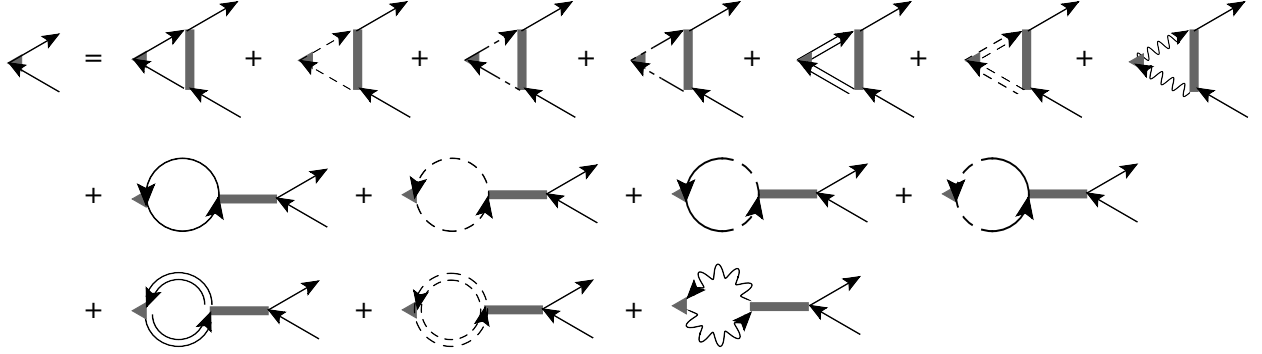


FIG. S9: Diagrammatic representation of the 1-loop renormalization of a representative Pomeranchuk vertex corresponding to the orbital density n_{xz} . The polarization bubbles are not logarithmic as they involve two identical propagators.

analysis is somewhat different than before because the polarization bubbles that renormalize the Pomeranchuk vertices are not logarithmically divergent as can be seen in Fig. S9. However, the scale-dependence of the interaction provides a logarithmic renormalization. Summing only logarithmic terms then leads to pRG equations in the Pomeranchuk channel of the form $\partial_L \Gamma_\mu \propto \Gamma_\mu^0 \partial_L u$, i.e. $\Gamma_\mu \propto \Gamma_\mu^0 (1 + u)$. Since the couplings flow as

$u \propto (L_0 - L)^{-1}$, the Pomeranchuk vertex grows with exponent $\beta_\mu = 1$ and overtakes the SC vertex at the end of the flow. Note however that the renormalization of the Pomeranchuk vertex develops when the couplings become of order one so that corrections to 1-loop RG may contribute. Explicitly the pRG equation of the Pomeranchuk channel for the toy model reads

$$\frac{d}{dL} \begin{pmatrix} \Gamma_{xz}^\Gamma \\ \Gamma_{yz}^\Gamma \\ \Gamma_{xy}^X \\ \Gamma_{xy}^Y \\ \Gamma_{xy}^M \end{pmatrix} = -2 \frac{d}{dL} \begin{pmatrix} u_4 & 0 & \frac{A_e}{A} (2u_1 - u_2) & \frac{A_e}{A} (2u_1 - u_2) & 0 \\ 0 & u_4 & \frac{A_e}{A} (2u_1 - u_2) & \frac{A_e}{A} (2u_1 - u_2) & 0 \\ \frac{A_h}{A} (2u_1 - u_2) & \frac{A_h}{A} (2u_1 - u_2) & u_5 & 0 & \frac{A_M}{A_n} (2u_{1n} - u_{2n}) \\ \frac{A_h}{A} (2u_1 - u_2) & \frac{A_h}{A} (2u_1 - u_2) & 0 & u_5 & \frac{A_M}{A_n} (2u_{1n} - u_{2n}) \\ 0 & 0 & \frac{A_e}{A_n} (2u_{1n} - u_{2n}) & \frac{A_e}{A_n} (2u_{1n} - u_{2n}) & u_{4n} \end{pmatrix} \begin{pmatrix} \Gamma_{xz}^\Gamma \\ \Gamma_{yz}^\Gamma \\ \Gamma_{xy}^X \\ \Gamma_{xy}^Y \\ \Gamma_{xy}^M \end{pmatrix}, \quad (\text{S30})$$

where we have omitted the irrelevant couplings (Eq. (S16)) and set $m_c = m_d$. As has been already obtained in Ref. [S4], the leading instability in the Pomeranchuk channel along the 4pFT is in the d-wave channel with non-equal densities $n_{xz} - n_{yz}$. Along the 3pFT an instability with different densities on the electron pocket

lets $n_{xy}(X) - n_{xy}(Y) \neq 0$ develops, which also breaks C_4 symmetry. Such an order splits one of the band degeneracies of the electron bands in the folded Brillouin zone.

Finally, we comment on the system behavior in a situation when the system does not reach a fixed trajec-

tory before the RG scale L becomes comparable to $L_F = \log \Lambda/E_F$. Because the susceptibility in the SDW channel is the largest over a wide range of L , it is most likely that in this situation the system develops an SDW order. We compared the behavior of SDW vertices involving fermions from one of the electron pockets and either fermions from Γ -centered hole pockets (Γ_{SDW}^Γ) or from the M -pocket (Γ_{SDW}^M). We found that $\Gamma_{SDW}^M > \Gamma_{SDW}^\Gamma$ if the flow is towards the 3pFT, and $\Gamma_{SDW}^\Gamma > \Gamma_{SDW}^M$ if the flow is towards the 4pFT. This implies that in the first case SDW order predominantly involves the triad of two electron pockets and the M hole pockets, while in the second case it involves two electron pockets and two Γ -centered hole pockets.

B. PRG for full 5-pocket model

1. PRG equations and fixed trajectories

We now move to the full 5-band model with xz/yz orbital content on the electron pockets. Like we said, in this case we have 19 more couplings (the total number of the couplings is 40). The couplings $\tilde{U}_4, \tilde{U}_4, \tilde{U}_5, \tilde{U}_5, U_a, U_b$ do not couple to additional terms and continue to flow to zero under pRG. We find six additional couplings $\tilde{V}_5, \tilde{V}_5, V_a, V_b, \bar{V}_a, \bar{V}_b$ that flow to zero. The corresponding pRG equations are

$$\begin{aligned} 4\pi \frac{d}{dL} (\tilde{V}_5 \pm \tilde{V}_5) &= -c_{pp}^{(4)} (\tilde{V}_5 \pm \tilde{V}_5)^2 \\ 4\pi \frac{d}{dL} (V_a \pm V_b) &= -c_{pp}^{(5)\pm} (V_a \pm V_b)^2 \\ 4\pi \frac{d}{dL} (\bar{V}_a \pm \bar{V}_b) &= -c_{pp}^{(6)} (\bar{V}_a \pm \bar{V}_b)^2, \end{aligned} \quad (\text{S31})$$

where $c_{pp}^{(4)} = 1/L \int d\omega \int d^2k G_{f_{31}, f_{31}} G_{f_{32}, f_{32}}$, $c_{pp}^{(5)\pm} = 1/L \int d\omega \int d^2k (G_{f_{31}, f_{31}} G_{f_1, f_1} \pm G_{f_{31}, f_1} G_{f_1, f_{31}})$, and $c_{pp}^{(6)} = 1/L \int d\omega \int d^2k G_{f_{31}, f_{31}} G_{f_2, f_2}$. For the other couplings we make the same conjecture as for the toy model, i.e., assume that for stable and weakly unstable fixed trajectories $U_i = \bar{U}_i, V_i = \bar{V}_i$. The one-loop RG equations for the remaining dimensionless couplings are

$$\begin{aligned} \dot{u}_1 &= u_1^2 + \frac{u_3^2}{a^2} \\ \dot{u}_{1n} &= u_{1n}^2 + \frac{u_{3n}^2}{a_n^2} \\ \dot{u}_2 &= 2u_2(u_1 - u_2) \\ \dot{u}_{2n} &= 2u_{2n}(u_{1n} - u_{2n}) \\ \dot{u}_3 &= 2u_3(2u_1 - u_2 - u_5) - 2bu_3u_4 - u_{3n}u_c \\ &\quad - 2v_3v_c - 2H(u_3v_c + v_3u_5) \\ \dot{u}_{3n} &= 2u_{3n}(2u_{1n} - u_{2n} - u_5) - u_{3n}u_{4n} - 2bu_3u_c \\ &\quad - 2v_{3n}v_c - 2H(u_{3n}v_c + v_{3n}u_5) \\ \dot{u}_4 &= -2bu_4^2 - 2u_3^2 - 2u_c^2 - 2v_3^2 - 4Hu_3v_3 \end{aligned}$$

$$\begin{aligned} \dot{u}_{4n} &= -u_{4n}^2 - 2u_{3n}^2 - 2bu_c^2 - 2v_{3n}^2 - 4Hu_{3n}v_{3n} \\ \dot{u}_5 &= -2u_5^2 - 2bu_3^2 - u_{3n}^2 - 2v_c^2 - 4Hu_5v_c \\ \dot{u}_c &= -2bu_4u_c - u_{4n}u_c - 2u_3u_{3n} \\ &\quad - 2v_3v_{3n} - 2H(v_3u_{3n} + v_{3n}u_3) \\ \dot{v}_1 &= v_1^2 + \frac{v_3^2}{c^2} \\ \dot{v}_{1n} &= v_{1n}^2 + \frac{v_{3n}^2}{c_n^2} \\ \dot{v}_2 &= 2v_2(v_1 - v_2) \\ \dot{v}_{2n} &= 2v_{2n}(v_{1n} - v_{2n}) \\ \dot{v}_3 &= 2v_3(2v_1 - v_2 - v_5) - 2bv_3u_4 - v_{3n}u_c \\ &\quad - 2u_3v_c - 2H(v_3v_c + u_3v_5) \\ \dot{v}_{3n} &= 2v_{3n}(2v_{1n} - v_{2n} - v_5) - v_{3n}u_{4n} - 2bv_3u_c \\ &\quad - 2u_{3n}v_c - 2H(v_{3n}v_c + u_{3n}v_5) \\ \dot{v}_5 &= -2v_5^2 - 2bv_3^2 - v_{3n}^2 - 2v_c^2 - 4Hv_5v_c \\ \dot{v}_c &= -2bv_3u_3 - 2v_5v_c - 2u_5v_c \\ &\quad - 2v_{3n}u_{3n} - 2H(v_c^2 + v_5u_5), \end{aligned} \quad (\text{S32})$$

where the additional parameters are

$$\begin{aligned} c &= \frac{\sqrt{A_h A'_e}}{A'} \quad c_n = \frac{\sqrt{A_M A'_e}}{A'_n} \quad H = \frac{A_e^a}{\sqrt{A_e A'_e}} \\ A_e &= \frac{1}{L} \frac{1}{(2\pi)^2} \int d\omega \int d^2k G_{f_1, f_1} G_{f_1, f_1} = m_e \int \frac{d\theta}{2\pi} \cos^4 \varphi_1 \\ A'_e &= \frac{1}{L} \frac{1}{(2\pi)^2} \int d\omega \int d^2k G_{f_{31}, f_{31}} G_{f_{31}, f_{31}} \\ &= m_e \int \frac{d\theta}{2\pi} \sin^4 \varphi_1 \\ A' &= \frac{1}{L} \frac{1}{(2\pi)^2} \int d\omega \int d^2k G_{f_{31}, f_{31}} G_{d_1, d_1} \\ &= 2 \int \frac{d\theta}{2\pi} \sin^2 \varphi_1 \left(\frac{m_c m_e}{m_c + m_e} \cos^2 \theta + \frac{m_d m_e}{m_d + m_e} \sin^2 \theta \right) \\ A'_n &= \frac{1}{L} \frac{1}{(2\pi)^2} \int d\omega \int d^2k G_{f_{31}, f_{31}} G_M \\ &= 2 \frac{m_M m_e}{m_M + m_e} \int \frac{d\theta}{2\pi} \sin^2 \varphi_1 \\ A_e^a &= \frac{1}{L} \frac{1}{(2\pi)^2} \int d\omega \int d^2k G_{f_1, f_1} G_{f_1, f_1} \\ &= m_e \int \frac{d\theta}{2\pi} \sin^2 \varphi_1 \cos^2 \varphi_1. \end{aligned} \quad (\text{S33})$$

Interestingly, we find that the stable fixed trajectories of the full model lead to the same decoupling at low-energies into effective three or four pocket models, as in the toy model. In distinction to the toy model, however, now there are two 3p and two 4p effective models ($3_1, 3_{p2}, 4_{p1}, 4_{p2}$). These four stable fixed trajectories are specified by

$$(4p_1) \quad u_i = \gamma_i u_1 \quad v_i = g_i u_1$$

$$\begin{aligned}
u_1 &= \frac{1}{1 + \gamma_3^2/a^2} \frac{1}{L_0 - L} \\
\gamma_3 &= \pm a \sqrt{8a^2 - 1 + 4\sqrt{1 - a^2 + 4a^4}} \\
\gamma_4 &= \gamma_5 = 1 - 2a^2 - \sqrt{1 - a^2 + 4a^4}
\end{aligned} \tag{S34}$$

(4p₂)

$$\begin{aligned}
u_i &= \gamma_i v_1 \quad v_i = g_i v_1 \\
v_1 &= \frac{1}{1 + g_3^2/c^2} \frac{1}{L_0 - L} \\
g_3 &= \pm c \sqrt{8c^2 - 1 + 4\sqrt{1 - c^2 + 4c^4}} \\
\gamma_4 &= g_5 = 1 - 2c^2 - \sqrt{1 - c^2 + 4c^4}
\end{aligned} \tag{S35}$$

(3p₁)

$$\begin{aligned}
u_i &= \gamma_i u_{1n} \quad v_i = g_i u_{1n} \\
u_{1n} &= \frac{1}{1 + \gamma_{3n}^2/a_n^2} \frac{1}{L_0 - L} \\
\gamma_{3n} &= \pm a_n \sqrt{4a_n^2 - 1 + 2\sqrt{4 - 2a_n^2 + 4a_n^4}} \\
\gamma_{4n} &= 2\gamma_5 = 2 - 2a_n^2 - \sqrt{4 - 2a_n^2 + 4a_n^4}
\end{aligned} \tag{S36}$$

(3p₂)

$$\begin{aligned}
u_i &= \gamma_i v_{1n} \quad v_i = g_i v_{1n} \\
v_{1n} &= \frac{1}{1 + g_{3n}^2/c_n^2} \frac{1}{L_0 - L} \\
g_{3n} &= \pm c_n \sqrt{4c_n^2 - 1 + 2\sqrt{4 - 2c_n^2 + 4c_n^4}} \\
g_{4n} &= 2g_5 = 2 - 2c_n^2 - \sqrt{4 - 2c_n^2 + 4c_n^4}
\end{aligned} \tag{S37}$$

All couplings not presented in the above formulas evolve with smaller exponents. Note that the ratios of the couplings in Eqs. (S34-S37) do not depend on the parameter H .

We see from Eqs. (S34-S35) that for 4p₁ and 4p₂ all interactions involving the M -centered hole pocket become subleading, like in the toy model. For 4pFT₁ the interactions involving xz/yz orbital components on the electron pockets become leading compared to the interactions involving xy orbital components, i.e., to first approximation the two electron pockets can be approximated as xz/yz -pockets. For 4p₂ the situation is opposite – the interactions involving xy orbital component on the electron pockets become dominant compared to the interactions involving xz/yz orbital components, i.e., to first approximation the two electron pockets can be approximated as xy pockets. These two fixed trajectories have been analyzed in Ref. [S4]. The situation is equivalent for the 3p₁ and 3p₂, see Eqs. (S36-S37). In the first case, the interactions involving xz/yz orbital component on the electron pockets become leading, and in the second the interactions involving xy orbital component on the electron pockets become leading.

These different effective low-energy models are sketched in Fig. 1 in the main text. We also note that the behavior of different couplings along 4p₁ and 4p₂ are quite similar, see Eqs. (S34, S35), and the same is true for the couplings along 3p₁ and 3p₂, Eqs. (S36,S37). Whether the system flows to 4p₁ or 4p₂ (or to 3p₁ or 3p₂) depends on the initial values of the couplings.

The stable FTs are separated by several weakly unstable ones with only a single direction along which perturbations grow. For general a, a_n, c, c_n , and H we determined these FTs and checked their stability numerically. For $a = a_n = c = c_n = 1$ these weakly unstable FTs can be analyzed analytically. The FTs with only one unstable direction are (the notations are self-evident):

(4p₁+4p₂)

$$\begin{aligned}
u_i &= \gamma_i u_1 \quad v_i = g_i u_1 \\
u_1 &= v_1 \quad u_3 = v_3 \quad u_5 = v_5 = v_c \\
u_1 &= \frac{1}{1 + \gamma_3^2/a^2} \frac{1}{L_0 - L} \\
\gamma_3 &= \pm \sqrt{15 + 16H + 4\sqrt{15 + 30H + 16H^2}} \\
\gamma_4 &= 2(H + 1)\gamma_5 = -3 - 4H\sqrt{15 + 30H + 16H^2}
\end{aligned} \tag{S38}$$

(3p₁+3p₂)

$$\begin{aligned}
u_i &= \gamma_i u_{1n} \quad v_i = g_i u_{1n} \\
u_{1n} &= v_{1n} \quad u_{3n} = v_{3n} \quad u_5 = v_5 = v_c \\
u_{1n} &= \frac{1}{1 + \gamma_{3n}^2/a_n^2} \frac{1}{L_0 - L} \\
\gamma_{3n} &= \pm \sqrt{7 + 8H + 4\sqrt{4 + 7H + 4H^2}} \\
\gamma_{4n} &= 4(H + 1)\gamma_5 = -2 - 4H - 2\sqrt{4 + 7H + 4H^2}
\end{aligned} \tag{S39}$$

(3p₁+4p₁)

$$\begin{aligned}
u_i &= \gamma_i u_1 \quad v_i = g_i u_1 \\
u_1 &= u_{1n} \quad u_3 = \pm u_{3n} \quad u_4 = u_{4n} = \pm u_c \\
u_1 &= \frac{1}{1 + \gamma_3^2/a^2} \frac{1}{L_0 - L} \\
\gamma_3 &= \sqrt{11 + 2\sqrt{34}} \quad \gamma_4 = -\frac{1}{3}(4 + \sqrt{34}) \\
\gamma_5 &= -2 - \sqrt{\frac{17}{2}}
\end{aligned} \tag{S40}$$

(3p₂+4p₂)

$$\begin{aligned}
u_i &= \gamma_i v_1 \quad v_i = g_i v_1 \\
v_1 &= v_{1n} \quad v_3 = \pm v_{3n} \quad u_4 = u_{4n} = \pm u_c \\
g_3 &= \sqrt{11 + 2\sqrt{34}} \quad \gamma_4 = -\frac{1}{3}(4 + \sqrt{34}) \\
g_5 &= -2 - \sqrt{\frac{17}{2}}.
\end{aligned} \tag{S41}$$

Again all couplings not listed in the formulas above have smaller exponents. A detailed analysis of the structure of weakly unstable FTs in the full 4-pocket model is presented in Ref. [S32].

Finally there is a high-symmetry FT with two unstable directions. Along this FT all couplings are non-zero:

$$\begin{aligned}
u_i &= \gamma_i u_1 & v_i &= g_i u_1 \\
u_1 &= u_{1n} = v_1 = v_{1n} & u_3 &= u_{3n} = v_3 = v_{3n} \\
u_4 &= h_{4n} = u_c & u_5 &= v_5 = v_c \\
u_1 &= \frac{1}{1 + \gamma_3^2/a^2} \frac{1}{L_0 - \bar{L}} \\
\gamma_3 &= \pm \sqrt{23 + 24H + 4\sqrt{34 + 69H + 36H^2}} \\
\gamma_4 &= \frac{4}{3}(H + 1)\gamma_5 = -\frac{10}{3} - 4H - \frac{2}{3}\sqrt{34 + 69H + 36H^2}.
\end{aligned} \tag{S42}$$

2. Susceptibilities

As in the toy model, we introduce vertices that couple to different order parameter fields to determine which order develops first at low energies. In the SDW channel, we now have four vertices

$$\begin{aligned}
\partial_L \Gamma_{SDW}^{\Gamma,1} &= \left(u_1 + \frac{u_3}{a}\right) \Gamma_{SDW}^{\Gamma,1} \\
\partial_L \Gamma_{SDW}^{\Gamma,2} &= \left(v_1 + \frac{v_3}{c}\right) \Gamma_{SDW}^{\Gamma,2} \\
\partial_L \Gamma_{SDW}^{M,1} &= \left(u_{1n} + \frac{u_{3n}}{a_n}\right) \Gamma_{SDW}^{M,1} \\
\partial_L \Gamma_{SDW}^{M,2} &= \left(v_{1n} + \frac{v_{3n}}{c_n}\right) \Gamma_{SDW}^{M,2}
\end{aligned} \tag{S43}$$

where indices 1,2 mean that the order parameters involve fermions on electron pockets with either $xz(yz)$ or xy orbital content, and indices Γ and M mean that the SDW order parameter involves fermions from either Γ -centered or M -centered hole pockets. Using the values of the couplings along the FTs as inputs and solving these differential equations, we obtain $\Gamma_{SDW}^{(i)} \sim 1/(L_0 - L)^{\beta_{SDW}^{(i)}}$, with $\beta_{SDW}^{(i)} = (1 + \gamma_{3i}/a_i)/(1 + \gamma_{3i}^2/a_i^2)$, where $i = (\Gamma, 1; \Gamma, 2; M, 1; M, 2)$ and $\gamma_{3i} \in \{\gamma_3, g_3, \gamma_{3n}, g_{3n}\}$, $a_i \in \{a, a_n, c, c_n\}$. We verified that *all* $\beta_{SDW}^{(i)}$ are smaller than 1/2, so that SDW order does not develop (if $L_0 < L_F$). The largest values are for $a = a_n = c = c_n = 1$: $\beta_{SDW}^{\Gamma,1} = \beta_{SDW}^{\Gamma,2} = 0.3$ and $\beta_{SDW}^{M,1} = \beta_{SDW}^{M,2} = 0.43$. These are the same values as in the toy model.

There are also four superconducting vertices: $\Gamma_{SC}^{e,xz/yz}$, $\Gamma_{SC}^{e,xy}$, Γ_{SC}^{Γ} , and Γ_{SC}^M . The RG equations

for these vertices can be cast into the matrix equation

$$\partial_L \mathbf{\Gamma}_{SC} = -2 \begin{pmatrix} u_5 + H v_c & v_c + H u_5 & u_3 & u_{3n} \\ v_c + H v_5 & v_5 + H v_c & v_3 & v_{3n} \\ u_3 + H v_3 & v_3 + H u_3 & u_4 & u_c \\ \frac{u_{3n} + H v_{3n}}{2} & \frac{v_{3n} + H u_{3n}}{2} & \frac{u_c}{2} & \frac{u_{4n}}{2} \end{pmatrix} \mathbf{\Gamma}_{SC}, \tag{S44}$$

where we introduced $\mathbf{\Gamma}_{SC} = (\Gamma_{SC}^{e,xz/yz}, \Gamma_{SC}^{e,xy}, \Gamma_{SC}^{\Gamma}, \Gamma_{SC}^M)^T$. Along each FT the solution of Eq. (S44) gives rise to s^{+-} gap structure on the contributing pockets. The exponents are

$$\begin{aligned}
\beta_{SC}^{(4p_1)} &= \frac{-\gamma_4 - \gamma_5 + \sqrt{(\gamma_4 - \gamma_5)^2 + 4\gamma_3^2}}{1 + \gamma_3^2/a^2} \\
\beta_{SC}^{(4p_2)} &= \frac{-\gamma_4 - g_5 + \sqrt{(\gamma_4 - g_5)^2 + 4g_3^2}}{1 + g_3^2/c^2} \\
\beta_{SC}^{(3p_1)} &= \frac{-\gamma_{4n} - 2\gamma_5 + \sqrt{(\gamma_{4n} - 2\gamma_5)^2 + 8\gamma_{3n}^2}}{1 + \gamma_{3n}^2/a_n^2} \\
\beta_{SC}^{(3p_2)} &= \frac{-\gamma_{4n} - 2g_5 + \sqrt{(\gamma_{4n} - 2g_5)^2 + 8g_{3n}^2}}{1 + g_{3n}^2/c_n^2}.
\end{aligned} \tag{S45}$$

For $a = a_n = c = c_n$ we have $\beta_{SC}^{(4p_1)} = \beta_{SC}^{(4p_2)} = 0.86$ and $\beta_{SC}^{(3p_1)} = \beta_{SC}^{(3p_2)} = 0.72$, again as in the toy model. We checked that $\beta_{SC}^{(i)} \geq 1/2$ for all a, a_n, c, c_n , i.e., the superconducting susceptibility does diverge at $L = L_0$.

To determine the SC gap structure on all pockets, we need to include the residual interactions. We did this numerically. We found that, like in the toy model, the largest eigenvalue in the SC channel corresponds to a "conventional" s^{+-} gap structure, although the magnitude of the gap on the "secondary" pockets is small. Specifically, this means that for $4p_1$ the gap magnitude is relatively small on the M -centered hole pocket and the xy -part of the electron pockets, for $4p_2$ it is small (very small) on the M -centered hole pocket and the xz/yz -parts of the electron pockets. In the $3p$ case, the gap almost vanishes on both Γ -centered hole pockets, and the two $3p$ FTs differ in the gap magnitude on the xz/yz and xy portions of the electron pockets.

For the second largest eigenvalue the gap structure for the FTs, where the dominant interactions are within the same orbitals (i.e. $4pFT_1$ and $3pFT_2$), is the orbital-antiphase s^{+-} state, Ref. [S29] ($\text{sign}(\Gamma_{SC}^{e,xz/yz}, \Gamma_{SC}^{e,xy}, \Gamma_{SC}^{\Gamma}, \Gamma_{SC}^M) = (+, -, -, +)$). For the FTs with dominant couplings between different orbitals ($4pFT_2$ and $3pFT_1$) the sign structure corresponds to "orbital-antiphase s^{++} " state ($\text{sign}(\Gamma_{SC}^{e,xz/yz}, \Gamma_{SC}^{e,xy}, \Gamma_{SC}^{\Gamma}, \Gamma_{SC}^M) = (+, -, +, -)$).